INS/GPS INTEGRATION AND ADAPTIVE FILTERING METHODS FOR GUIDED MUNITIONS

A THESIS SUBMITTED TO
THE GRADUATE SCHOOL OF NATURAL AND APPLIED SCIENCES
OF
MIDDLE EAST TECHNICAL UNIVERSITY

BY

NUR SILA EROĞLU

IN PARTIAL FULFILLMENT OF THE REQUIREMENTS
FOR
THE DEGREE OF MASTER OF SCIENCE
IN
AEROSPACE ENGINEERING

SEPTEMBER 2023

Approval of the thesis:

INS/GPS INTEGRATION AND ADAPTIVE FILTERING METHODS FOR GUIDED MUNITIONS

submitted by **NUR SILA EROĞLU** in partial fulfillment of the requirements for the degree of **Master of Science** i**n Aerospace Engineering, Middle East Technical University** by,

Prof. Dr. Halil Kalıpçılar
Dean, Graduate School of **Natural and Applied Sciences** _____

Prof. Dr. Serkan Özgen
Head of the Department, **Aerospace Engineering** _____

Assoc. Prof. Dr. Halil Ersin Söken
Supervisor, **Aerospace Engineering** _____

Examining Committee Members:

Prof. Dr. Ozan Tekinalp
Aerospace Engineering, METU _____

Assoc. Prof. Dr. Halil Ersin Söken
Aerospace Engineering, METU _____

Assoc. Prof. Dr. Mustafa Mert Ankaralı
Electrical and Electronics Engineering, METU _____

Asst. Prof. Dr. Ali Türker Kutay
Aerospace Engineering, METU _____

Asst. Prof. Dr. Tuncay Yunus Erkeç
Atasaren, NDU _____

Date: 11.09.2023

I hereby declare that all information in this document has been obtained and presented in accordance with academic rules and ethical conduct. I also declare that, as required by these rules and conduct, I have fully cited and referenced all material and results that are not original to this work.

Name Last name : Nur Sıla Eroğlu

Signature :

ABSTRACT

INS/GPS INTEGRATION AND ADAPTIVE FILTERING METHODS FOR GUIDED MUNITIONS

Eroğlu, Nur Sıla
Master of Science, Aerospace Engineering
Supervisor: Assoc. Prof. Dr.Halil Ersin Söken

September 2023, 81 pages

INS/GPS integration is a widely used application in aerospace to obtain navigation solutions. Both sensors have complementing properties, and navigation solution improves significantly when INS and GPS are utilized together. This study applies INS/GPS integration on a guided munition by loosely and tightly coupled integration techniques. Error-state Kalman filters are used in INS/GPS integration. Even though GPS provides measurements with high precision, GPS can be prone to outside effects, and the measurements from GPS can become unreliable. For these situations, adaptive Kalman filter is implemented. This adaptive method calculates scale factors for the measurement noise covariance matrix. If a faulty measurement is detected, these scale factors are multiplied with the measurement noise covariance matrix. Scale factors can be singular (SSF) or multiple (MSF), meaning it can be a scalar or a diagonal matrix. It is illustrated that MSF helps to obtain better navigation solutions in all cases compared to the faulty measurement and SSF. On the other SSF provides better navigation solutions in several cases than the faulty measurement. It is concluded that if GPS measurements are faulty, using MSF adaptive Kalman filter helps to obtain better navigation solutions for a guided munition.

Keywords: INS/GPS Integration, Loosely Coupled, Tightly Coupled, Adaptive Kalman Filters, Guided Munitions

ÖZ

GÜDÜMLÜ MÜHİMMATLAR İÇİN ANS/KKS TÜMLEŞTİRİLMESİ VE ADAPTİF FİLTRELEME YÖNTEMLERİ

Eroğlu, Nur Sıla
Yüksek Lisans, Havacılık ve Uzay Mühendisliği
Tez Yöneticisi: Doçent Dr.Halil Ersin Söken

Eylül 2023, 81 sayfa

ANS/KKS tümleştirilmesi, navigasyon çözümleri elde etmek için havacılık ve uzay sektöründe yaygın olarak kullanılan bir uygulamadır. Sensörler birbirlerini tamamlayıcı özelliğe sahiptir ve ANS ve KKS birlikte kullanıldığında navigasyon çözümü önemli ölçüde gelişir. Bu çalışmada gevşek tümleştirilmiş ve sıkı tümleştirilmiş ANS/KKS tümleştirilmeleri güdümlü mühimmatlar üzerinde uygulanmıştır. Hata durumlu Kalman filtresi ANS/KKS tümleştirilmesinde kullanılmıştır. KKS yüksek hassasiyette ölçümler sağlasa da dış etkilere açık olabilir ve KKS ölçümleri güvenilmez hale gelebilir. Bu durumlar için adaptif Kalman filtresi uygulanmıştır. Bu adaptif yöntem ölçüm gürültüsü kovaryans matrisi için ölçek çarpanları hesaplar. Eğer hatalı bir ölçüm tespit edilirse, ölçek çarpanları ölçüm gürültüsü kovaryans matrisi ile çarpılır. Ölçek çarpanları tekil veya çoklu olabilir. Tüm durumlarda çoklu çarpanın hatalı ölçüm durumuna veya tekil çarpana göre daha iyi navigasyon çözümü ürettiği gösterilmiştir. Bazı durumlarda ise tekil çarpan hatalı duruma göre daha iyi sonuç verir. Sonuç olarak KKS ölçümleri hatalıysa, çoklu ölçek çarpanlı adaptif Kalman filtresi güdümlü bir mühimmat için daha iyi navigasyon sonuçları elde edilmesine yardımcı olur.

Anahtar Kelimeler: ANS/KKS Tümleştirilmesi, Gevşek Tümleştirilmiş, Sıkı Tümleştirilmiş Adaptif Kalman Filtreleri, Güdümlü Mühimmatlar

To all women who persist, inspire, and pave the way for equality

ACKNOWLEDGMENTS

I am profoundly grateful to my advisor, Assoc. Prof. Dr. Halil Ersin Söken for his exceptional guidance and mentorship. He demonstrated a rare combination of expertise and patience, always taking the time to discuss and refine my ideas, contributing immensely to the quality of this thesis.

I am thankful to my company, Roketsan Missiles Inc., for their support and the invaluable opportunities provided during the completion of my thesis. I am sincerely grateful to my esteemed colleague, Haydar Tolga Avcıoğlu, whose wealth of experience and wisdom has been an invaluable inspiration to my professional growth. I would like to thank my colleagues and friends Emre Han Ata, Cansu Yıldırım, and Elif Koç. Your technical expertise and willingness to help have been invaluable.

I would like to extend my heartfelt appreciation to my best friends, Suzan Kale Güvenç, Berna Ünal, and Naz Tuğçe Öveç. I am fortunate to have friends who are not only willing to share their knowledge but also stand by me with enthusiasm and genuine friendship. I am thankful to Tutku Ilgın Özcan for her ability to turn the most stressful moments into fun experiences. Your friendship is a treasure beyond measure.

I want to extend my heartfelt gratitude to my dear brother, Halil İbrahim Eroğlu, whose lasting encouragement has been a constant source of strength and motivation throughout the journey of completing this thesis.

Finally, I extend my deepest gratitude to my incredible family – my mom, Selda Eroğlu; my dad, Adnan Rüştü Eroğlu; and my little brothers, İsmail Çağrı Eroğlu, and Muhsin Efe Eroğlu. To my mom and dad, your sacrifices and endless encouragement have been the driving force behind my pursuit of knowledge. Your belief in my abilities, even when I doubted myself, has given me the strength to persevere. To my little brothers, your presence has added warmth and light to even the most challenging moments.

TABLE OF CONTENTS

LIST OF TABLES

TABLES

LIST OF FIGURES

FIGURES

LIST OF ABBREVIATIONS

AKF: Adaptive Kalman Filter

DCM: Direction Cosine Matrix

GNSS: Global Navigation Satellite System

GPS: Global Positioning System

IMU: Inertial Measurement Unit

INS: Inertial Navigation System

KF: Kalman Filter

MSF: Multiple Scale Factor

PNG: Proportional Navigation Guidance

SSF: Single Scale Factor

wrt: with respect to

LIST OF SYMBOLS

α: angle of attack

a_{com}^{n}: acceleration command resolved in the navigation frame

a_{com}^{b}: acceleration command resolved in the body frame

b_g: bias of accelerometer

b_g: bias of gyroscope

b_{GNSS}^{m}: clock bias of satellite number-m

β: sideslip angle

$\bar{\beta}$: reduced latitude

C_b^e: DCM that transforms a vector from the body frame to the earth frame

C_e^n: DCM that transforms a vector from earth frame to navigation frame

C_b^n: DCM that transforms a vector from body frame to navigation frame

C_L: aerodynamic moment coefficient in the body x direction

C_{l_p}: change in l-moment coefficient wrt the change in p

C_M: aerodynamic moment coefficient in the body z direction

$C_{m_{\dot{\alpha}}}$: change in m-moment coefficient wrt the change in $\dot{\alpha}$

C_{m_q}: change in m-moment coefficient wrt the change in q

C_N: aerodynamic moment coefficient in the body y direction

$C_{n_{\dot{\beta}}}$: change in n-moment coefficient wrt the change in $\dot{\beta}$

C_{n_r}: change in n-moment coefficient wrt the change in r

C_X: aerodynamic force coefficient in the body x direction

C_Y: aerodynamic force coefficient in the body y direction

C_Z: aerodynamic force coefficient in the body z direction

C_{z_q}: change in z-force coefficient wrt the change in q

δx: error-state vector

e: eccentricity of the earth

ε_a: noise of accelerometer

ε_g: noise of gyroscope

$\tilde{\varepsilon}_{GNSS}^{m}$: total effect of residual errors for satellite number-m

f: flatness of the earth

f_{ib}^{b}: specific force of the body resolved in the body frame

f_{ib}^{n}: specific force of the body resolved in the navigation frame

F: dynamic coefficient matrix

F^b: aerodynamic force vector resolved in the body frame

g^b: gravity vector resolved in the body frame

h: altitude

I^b: body inertia matrix

1_{LOS}^{m}: line-of-sight unit vector for satellite number-m

$\mathrm{L_{ref}}$: reference length

λ: longitude

m: mass of the guided munition

M: Mach number

M^b: aerodynamic moment vector resolved in the body frame

N_{PNG}: proportional navigation guidance gain

ω_e: Earth's angular rotation velocity

ω_{en}^{n}: earth angular rate wrt navigation frame resolved in the navigation frame

ω_{ie}^{e}: earth angular rate wrt inertial frame resolved in the earth frame

ω_{ib}^{b}: body angular rate wrt inertial frame resolved in body frame

ω_{LOS}: line-of-sight angular rate between target and body

ω_{nb}^{b}: body angular rate wrt navigation frame resolved in body frame

p: body angular rate in the body x direction

φ: latitude

q: body angular rate in the body z direction

Q: dynamic pressure

r: body angular rate in the body y direction

r^m: true distance between the GNSS receiver and the satellite number-m

R: radius of the earth

R_N: the radius curvature of the prime vertical

R_M: the meridian radius of curvature

ρ_{GNSS}^{m}: pseudo-range measurement from satellite number-m

$\dot{\rho}_{GNSS}^{m}$: pseudo-range rate measurement from satellite number-m

r_{eb}^{e}: position of the body wrt earth resolved in the earth frame

r_{GNSS}^{m}: satellite number-m's position resolved in the earth frame

s: square of the first eccentricity

S_{ref}: reference area

V: magnitude of the body velocity vector

v_{eb}^{b}: velocity of the body wrt earth resolved in body frame

v_{eb}^{e}: velocity of the body wrt earth resolved in the earth frame

v_{eb}^{n}: velocity of the body wrt earth resolved in the navigation frame

v_{GNSS}^{m}: velocity of satellite number-m resolved inearth frame

CHAPTER 1

INTRODUCTION

1.1 Motivation

INS/GNSS integration is applied for many aerospace applications to have better navigation solutions. INS and GNSS both have their advantages and disadvantages. However, if they are utilized together, they can offer better navigation solutions. INS/GNSS integration can be achieved with different tools and integration methods. One of the widely used tools is the Kalman filter, which is implemented in this study. Both loosely coupled and tightly coupled integration methods are adapted. For guided munition applications, even though INS/GNSS can be helpful, GNSS can be prone to spoofing, which results in faulty measurements. In this case, one way can be rejecting the faulty measurement and using only INS update for the navigation solutions. On the other hand, an adaptive Kalman filter can be applied to decrease the faulty measurement effect while still using valuable measurements from GNSS. This thesis aims to show that in the case of GNSS spoofing, an adaptive Kalman filter can provide a better navigation solution instead of using INS update only in some scenarios.

1.2 Literature Review

Precision guided munition's definition is a guided weapon with the purpose of exterminating a target and also decreasing unwanted casualties, according to [1]. PGMs were introduced in WW II; however, their operational use was in the Vietnam War [2]. They can be categorized as air-launched, ground-launched, and naval-launched. PGMs use INS, GNSS, and laser guidance [2]. In this study, an air-

launched PGM with no thrust, which has the INS and GNSS receiver is the point of interest. INS and GNSS receiver are two important components of the guided munition. INS is composed of three mutually orthogonal accelerometers, three mutually orthogonal gyroscopes, and a navigation processor [3], [4], [5]. Accelerometers measure the specific force, which is the acceleration of the body minus the gravity in that direction. Gyroscopes measure the angular rate of the body with respect to the inertial frame. While accelerometers and gyroscopes provide the specific force and angular rate, the navigation processor calculates the position, velocity, and attitude of the body, which will be used in guidance and autopilot algorithms of the guided munition.

INS is utilized in most aerospace vehicles because it is a dead-reckoning system, meaning it does not need external references [3], [4]. INS calculates orientation and position by integrating the measurements with a known initial condition. However, this introduces a disadvantage of accumulating errors with time [5]. INS provides a navigation solution in high frequency, at least 50 Hz, according to [5]. GNSS includes the constellation of satellites orbiting the Earth, which helps a vehicle with a receiver to calculate its position and velocity. Some examples of GNSS constellations are GPS, GLONASS, and Galileo. The most used constellation is GPS, which belongs to the United States; GLONASS belongs to Russia, and Galileo belongs to the European Union [3]. These satellites transmit signals with the information of their position, velocity, and the exact time that the signal is sent. The vehicle with the GNSS receiver uses this signal to obtain its position and velocity from at least four different satellites [3], [4]. One of the advantages of GNSS is that it can provide positionforbita and velocity with high accuracy for the long term. However, the measurement frequency is low compared to INS, typically between 1-10 Hz [6]. Another disadvantage of GNSS is that it is highly affected by outside conditions. These conditions can block the signal transmitted, or some interference from other signal sources can occur. This is where INS/GNSS integration could be beneficial. Both INS and GNSS have their advantages and disadvantages when both of their measurements are utilized, better navigation solutions could be provided.

INS/GNSS integration could be categorized according to the coupling degree between them, which are loosely coupled, tightly coupled, and ultra-tightly coupled integration. While loosely coupled and tightly coupled integration are the points of interest of this study, ultra-tightly coupled integration is not. GNSS receivers can provide measurements in different ways, such as direct position and velocity or pseudorange and pseudorange-rate measurements. If position and velocity solutions from the GNSS receiver are used directly, loosely coupled integration is adapted [3]. If pseudorange and pseudorange-rate measurements are used, then tightly coupled INS/GNSS integration is applied [3]. In the case of pseudorange and pseudorange-rate estimations, they are fed back to the GNSS receiver's tracking loop, and then an ultra-tightly coupled integration method is utilized [3].

INS/GNSS integration can be achieved by using different tools such as Kalman filters and particle filters. Particle filters can be beneficial in case of non-Gaussian noise distribution. On the other hand, Kalman filters are optimal estimators for the Gaussian noise characteristics. The particle filter and Kalman filter are compared in [7]; while the particle filter provides a robust trajectory, the Kalman filter has shorter computation time. Kalman filters are widely used in INS/GNSS integration literature. The main types of Kalman filters used in INS/GNSS integration are linearized Kalman filters, extended Kalman filters, and unscented Kalman filters, also known as sigma-point Kalman filters. These Kalman filters differ in system and measurement models and their computational loads. Linear KF is an optimal estimator for linear systems. Since all systems are nonlinear in real-life navigation applications, using linear systems and measurement models may not be preferable for certain reasons. In this case, extended KFs can be introduced. Nonlinear systems or measurement models can be linearized using Taylor series expansion around the estimated state vector [8]. An EKF is used for INS/GPS navigation systems in [9], because of the nonlinear dynamics of GPS measurements. However, when a GPS outage exists, the algorithm switches to the linear KF. Unscented KF guesses the random variable statistics using sigma points [8]. The results in [8] illustrate that

UKF has better performance than EKF to some degree. On the other hand, the computational load that UKF brings compared to EKF is higher [8].

KF applications vary in using full-state or error-state in its system and measurement model. Error state utilization is possible with small perturbation theory. By using the error-state, equations become linear, and optimal KF can be achieved [10]. One major drawback of using error-state is that the errors due to linearization can grow with time. Due to the relatively short time of flight of the guided munition, an error-state extended Kalman filter is applied in this thesis. In [11], a tightly coupled INS/GPS integration is applied for a guided munition. Different trajectories are studied in [11]; short range trajectories have some problems because of lack of time sufficient for INS calibration and alignment. INS/GPS tightly and deeply integration are applied on guided munition, and their performances are compared under GPS jamming in [12]. It turns out deeply integration architecture has better performance compared to tightly coupled integration.

As stated before, GNSS is prone to suffer from outside effects such as spoofing and jamming. The measurements from GNSS are tested to detect any malfunction. One solution to this problem is using INS update only and rejecting the GNSS measurements. Another solution is that utilizing adaptive KFs. In [13], adaptive Kalman filters, which are multiple-model-based adaptive estimation (MMAE) and innovation-based adaptive estimation (IAE), are reviewed. MMAE has different KFs running at the same time with different process noise and/or measurement noise matrices. In the beginning, all KFs have the same weight factor. After a while, MMAE learns which KF has better noise matrices, and its weighting factor increases while others go to zero [13]. On the other hand, by using statistical information, theoretical values for process and measurement covariance matrices are calculated and adapted throughout the process [13]. The adaptive KF method used in this thesis is innovation-based R-adaptation applied from [14]. This method includes calculating a scale factor to multiply with the measurement noise covariance matrix. According to the designer's choice, this scale factor can be single or multiple. The measurement noise covariance matrix is adapted if there is a malfunction in the

measurements. This malfunction can be detected with different methods. In this thesis, integrity monitoring is achieved by using the chi-square test.

CHAPTER 2

PRELIMINARIES

2.1 Reference Frames

Reference frames are used to indicate relative positions or velocities of vectors [15]. In navigation, relative frame descriptions are important for mechanization equations. The reference frames utilized in this thesis are given in the following subsections.

2.1.1 Earth-Centered Inertial Frame

An inertial frame should be non-rotating and have a fixed origin. For navigation purposes, the earth-centered inertial frame is used. Although Earth's orbit has a centripetal acceleration, it is assumed to be negligible [5]. The origin of the inertial frame coincides with the center of mass of the Earth. The z-axis of the Earth-centered inertial frame is towards the north pole. The x-axis and y-axis lie on the equatorial plane, while the x-axis is to the vernal equinox; the y-axis completes the right-handed coordinate system.

2.1.2 Earth-Centered Earth-Fixed Frame

The earth-fixed frame rotates with the Earth. However, it has the same origin and z-axis as the inertial frame [4]. The x-axis of the Earth-fixed frame is towards the intersection point between the Greenwich meridian and the equatorial plane. The y-axis completes the right-handed coordinate system. Both the inertial frame and Earth-fixed frame are illustrated in Figure 2-1. Where ω_e states the Earth's angular rotation velocity.

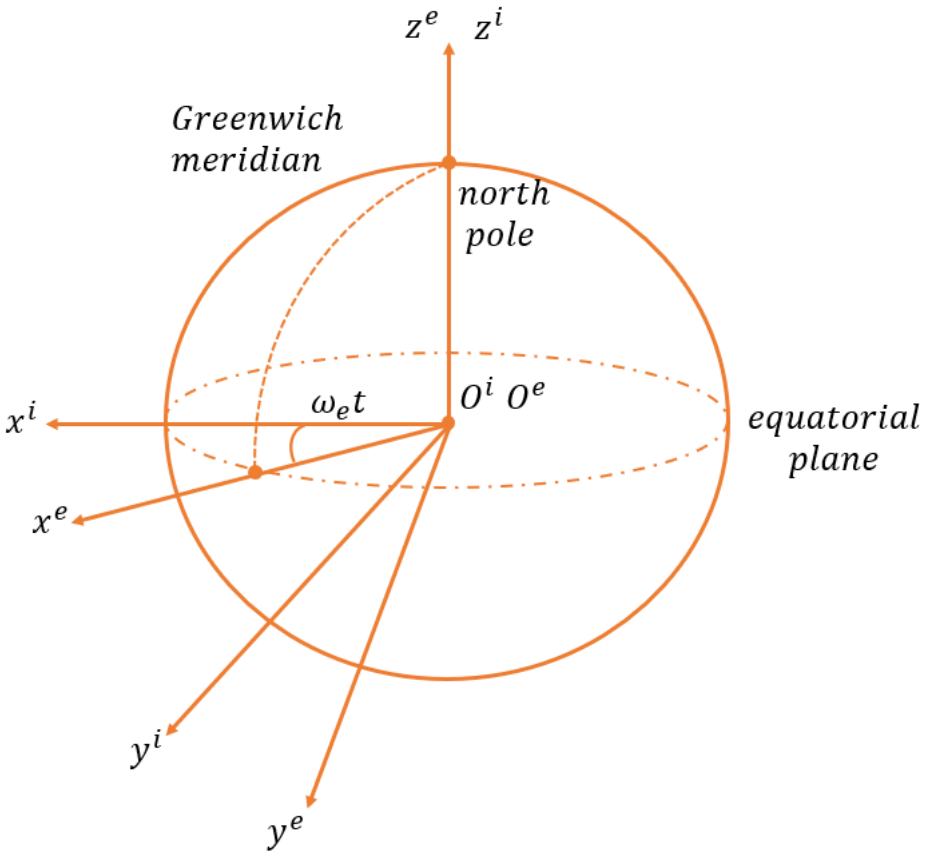

Figure 2-1. Earth-Centered Inertial Frame and Earth-Centered Earth-Fixed Frame

2.1.3 Navigation Frame

The navigation frame has its origin at the IMU location, even though, in some applications, it can be placed at the center of mass [5]. The z-axis of the navigation frame, which is referred to as down, points to the center of the Earth. Gravity is assumed to be in the z-axis [4]. The x-axis of the frame points to the North Pole and is referred to as North. The y-axis completes the right-handed coordinate system, which results in pointing East. Throughout this thesis, the navigation frame may be referred to as the NED-frame (North-East-Down).

2.1.4 Body Frame

The body frame has its origin at the IMU location, which coincides with the navigation frame's origin. The x-axis points to the nose of the guided munition, while the y-axis points to the right side of the guided munition. The z-axis completes the right-handed coordinate system. Both the navigation frame and body frame are illustrated in Figure 2-2.

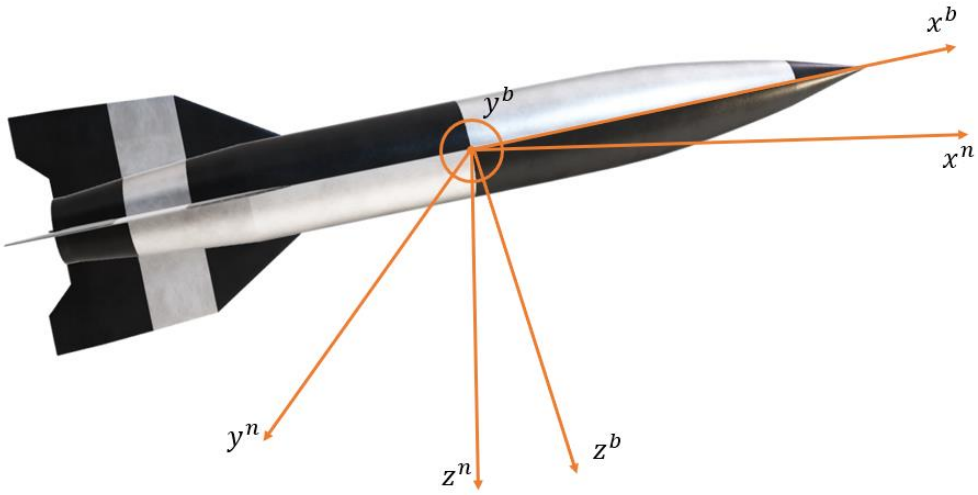

Figure 2-2. Navigation Frame and Body Frame

2.2 Reference Frame Transformations

Vectors have different representations in different reference frames. In navigation, these representations are needed because measurements are provided in different frames. The direction cosine matrices (DCMs) are created according to the rotation angle and rotation axis for a vector to have a representation in another reference frame. Sometimes, more than one rotation is needed to obtain the vector representation from one frame to the other. Multiplying the matrices is a way of creating the overall DCM. An important and useful property of the DCM is that the inverse of the DCM is equal to its transpose [3].

2.2.1 Euler Angles

One frame's orientation can be obtained by applying three rotations around the z, y, and x axes of another frame. In aerospace applications, Euler angles are defined as three angles that are obtained by rotation from the navigation frame to the body frame. The rotations are explained below and illustrated in Figure 2-3, Figure 2-4, and Figure 2-5.

1) The first rotation is around the z-axis of the navigation frame, and the angle is denoted by ψ.

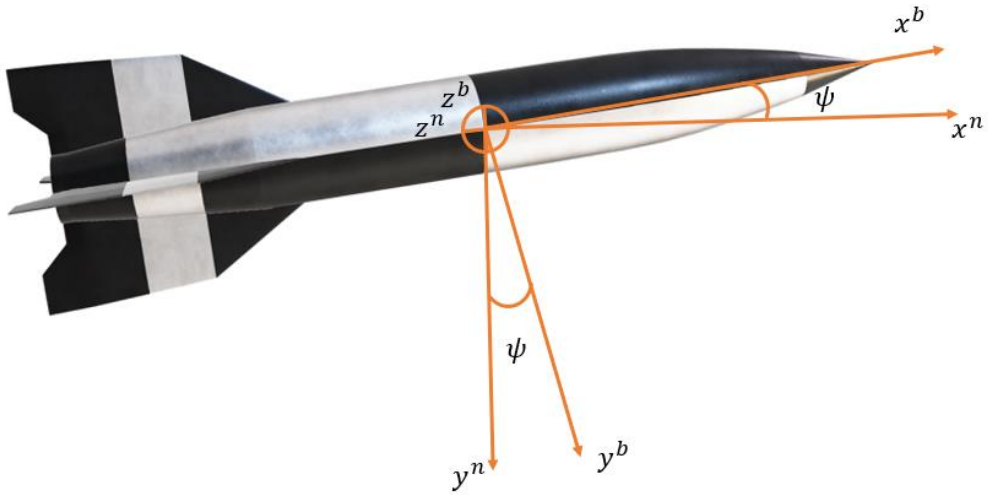

Figure 2-3 Euler Angles – First Rotation -The Top View

2) The second rotation is around the y-axis of the new frame obtained after the first rotation and denoted by θ.

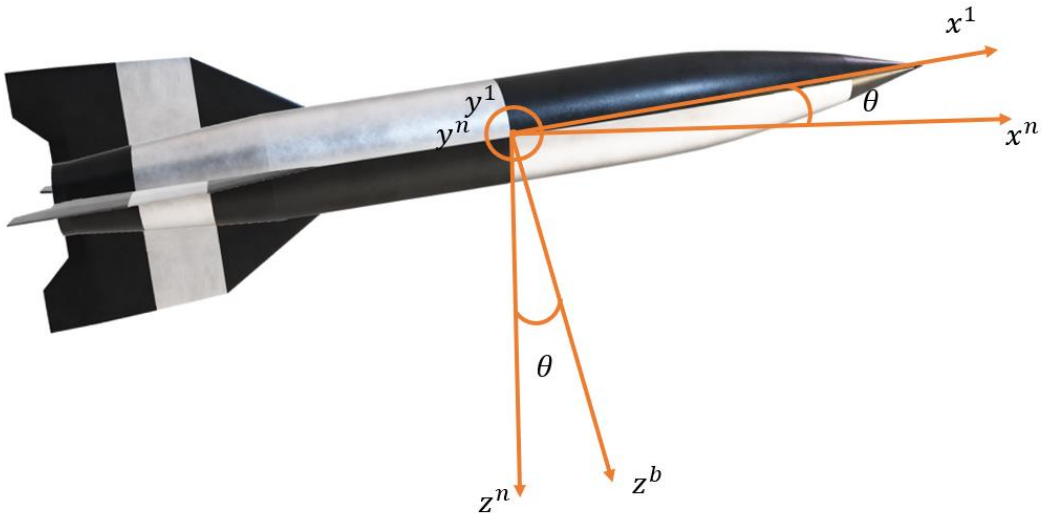

Figure 2-4 Euler Angles – Second Rotation -The Side View

3) The third rotation is around the x-axis of the new frame obtained after the second rotation and denoted by ϕ.

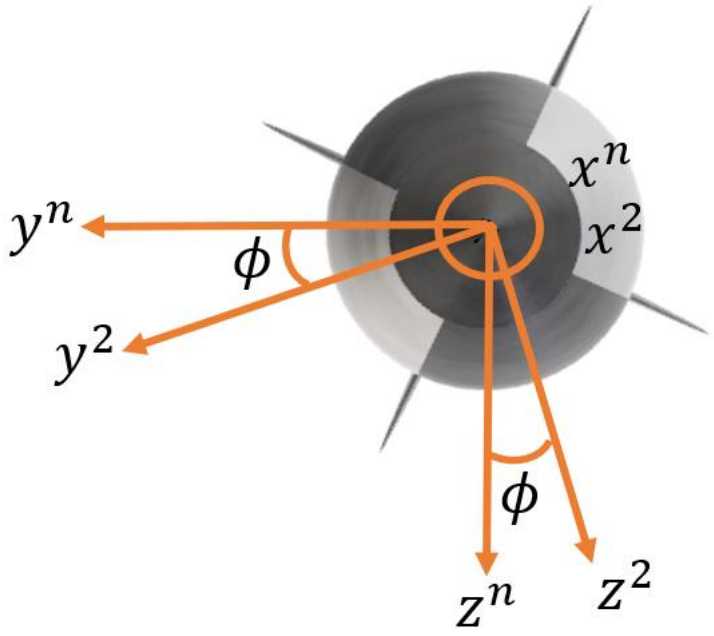

Figure 2-5 Euler Angles – Third Rotation – The Front View

2.2.2 Transformation From Inertial Frame to Earth-Fixed Frame

As stated in Chapter 2.1.2, Earth-fixed frame and inertial frame have the same origin and share their z-axes. Therefore, a rotation matrix around the z-axis, including the Earth's rotation rate multiplied with time, is sufficient for the transformation from an inertial frame to an Earth-fixed frame [3].

$$C_i^e = \begin{bmatrix} \cos \omega_e t & \sin \omega_e t & 0 \\ -\sin \omega_e t & \cos \omega_e t & 0 \\ 0 & 0 & 1 \end{bmatrix} \tag{2.1}$$

$$C_e^i = (C_i^e)^T \tag{2.2}$$

2.2.3 Transformation From Earth-Fixed Frame to Navigation Frame

The earth frame and navigation frame are illustrated in Figure 2-6. The first rotation for the transformation of the Earth frame to the navigation frame is around the z-axis and by the angle longitude. The second rotation is around the y-axis and by $90°$. The final rotation is around the z-axis and by the angle of longitude.

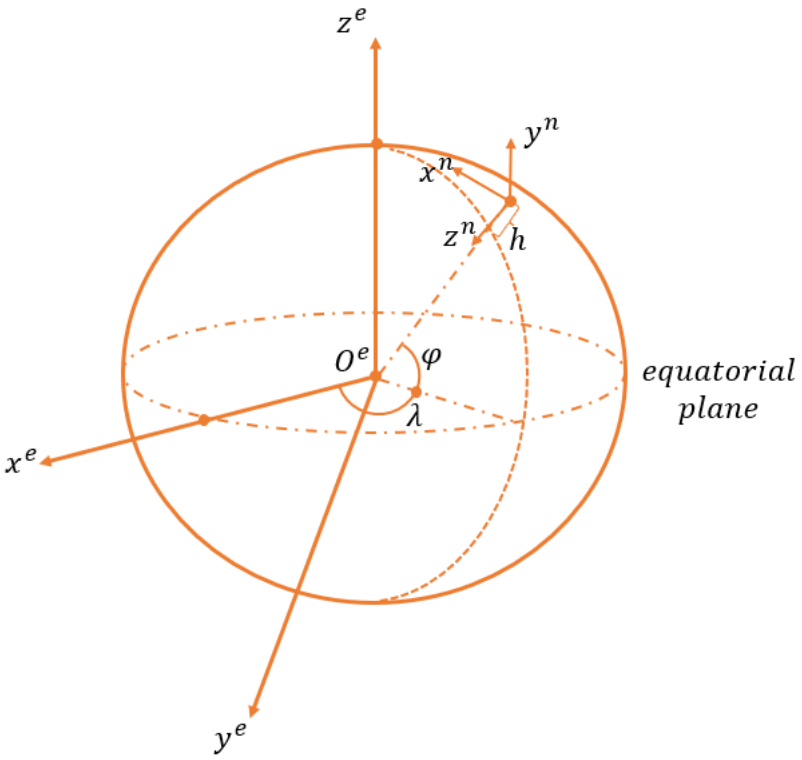

Figure 2-6. Earth Frame and Navigation Frame

DCM that transforms a vector from the Earth frame to the navigation frame is created by multiplying three rotation matrices and given as in Eq. (2.3) and as stated in [16].

$$C_e^n = \begin{bmatrix} \cos\varphi & 0 & \sin\varphi \\ 0 & 1 & 0 \\ -\sin\varphi & 0 & \cos\varphi \end{bmatrix} \begin{bmatrix} 0 & 0 & 1 \\ 0 & 1 & 0 \\ -1 & 0 & 0 \end{bmatrix} \begin{bmatrix} \cos\lambda & \sin\lambda & 0 \\ -\sin\lambda & \cos\lambda & 0 \\ 0 & 0 & 1 \end{bmatrix} \tag{2.3}$$

$$C_e^n = \begin{bmatrix} -sin\varphi\cos\lambda & -sin\varphi\sin\lambda & \cos\varphi \\ -\sin\lambda & \cos\varphi & 0 \\ -\cos\varphi\cos\lambda & -\cos\varphi\sin\lambda & -\sin\varphi \end{bmatrix} \tag{2.4}$$

$$C_n^e = (C_e^n)^T \tag{2.5}$$

2.2.4 Transformation From Navigation Frame to Body Frame

The transformation from the navigation frame to the body frame is achieved by Euler angles, which are explained in detail in Chapter 2.2.1. The DCM is created by

multiplying three rotation matrices utilizing the Euler angles as given in Eq. (2.6) as stated in [16]. As explained before, the rotation sequence is z, y, and x axes, which also can be referred to as 3-2-1 rotation.

$$C_n^b = \begin{bmatrix} 1 & 0 & 0 \\ 0 & \cos\phi & \sin\phi \\ 0 & -\sin\phi & \cos\phi \end{bmatrix} \begin{bmatrix} \cos\theta & 0 & -\sin\theta \\ 0 & 1 & 0 \\ \sin\theta & 0 & \cos\theta \end{bmatrix} \begin{bmatrix} \cos\psi & \sin\psi & 0 \\ -\sin\psi & \cos\psi & 0 \\ 0 & 0 & 1 \end{bmatrix} \quad (2.6)$$

$$C_n^b = \begin{bmatrix} \cos\theta\cos\psi & \cos\theta\sin\psi & -\sin\theta \\ -\cos\phi\sin\psi + \sin\phi\sin\theta\cos\psi & \cos\phi\cos\psi + \sin\phi\sin\theta\sin\psi & \sin\phi\cos\theta \\ \sin\phi\sin\psi + \cos\phi\sin\theta\cos\psi & -\sin\phi\cos\psi + \cos\phi\sin\theta\sin\psi & \cos\phi\cos\theta \end{bmatrix} \quad (2.7)$$

$$C_b^n = (C_n^b)^T \quad (2.8)$$

2.3 The Deflection Angle Representation

In conventional air vehicles, primary deflection angles are aileron, elevator, and rudder, which are responsible for the control of the vehicle's roll, pitch, and yaw motion [16]. Guided munitions can have front or rear control surfaces. In this study, the guided munition has rear control surfaces called tail fins, as illustrated in Figure 2-7 [17]. To understand the effect of the control surfaces on the guided munition, the representation of the conventional control surfaces in terms of tail fin deflections is given in Eq. (2.9), (2.10), and (2,11).

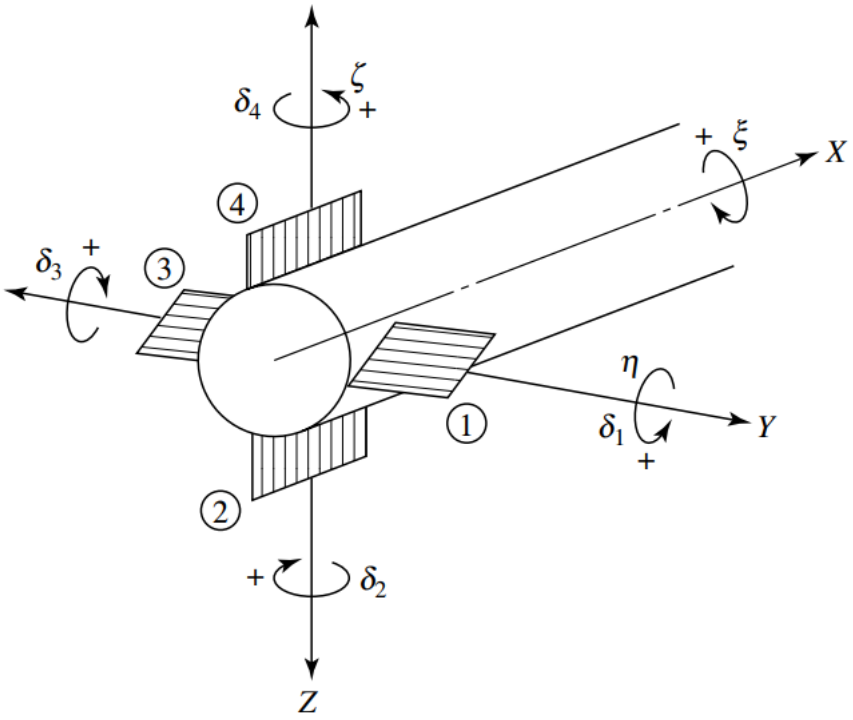

Figure 2-7: Tail Control Surfaces [16]

$$\delta_a = \frac{1}{4}(\delta_1 + \delta_2 + \delta_3 + \delta_4) \tag{2.9}$$

$$\delta_r = \frac{1}{2}(\delta_2 - \delta_4) \tag{2.10}$$

$$\delta_e = \frac{1}{2}(\delta_1 - \delta_3) \tag{2.11}$$

CHAPTER 3

METHODOLOGY

3.1 6-DOF Simulation Model of The Guided Munition

A simulation model is created to analyze the dynamics of the guided munition within Matlab-Simulink. The model has two main parts: one part is the real world, and the other part is the guided munition part, as can be observed from Figure 3-1.

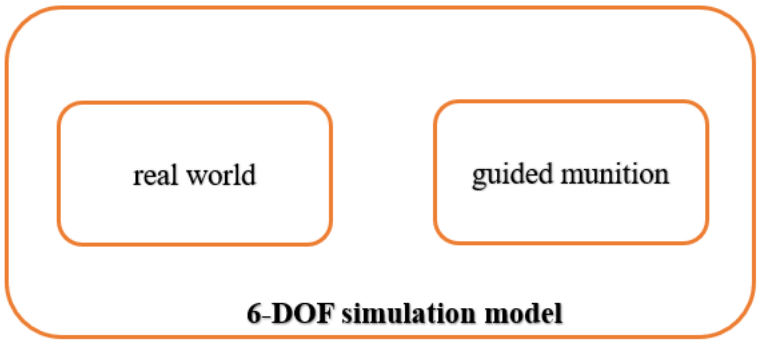

Figure 3-1. 6-DOF Simulation Model Representation

In the real world part, environment, aerodynamics, and equations of motion are modeled. In the guided munition part, avionics, navigation, autopilot, and guidance are modeled. For both parts, relationships between their subparts are illustrated in Figure 3-2 and Figure 3-3.

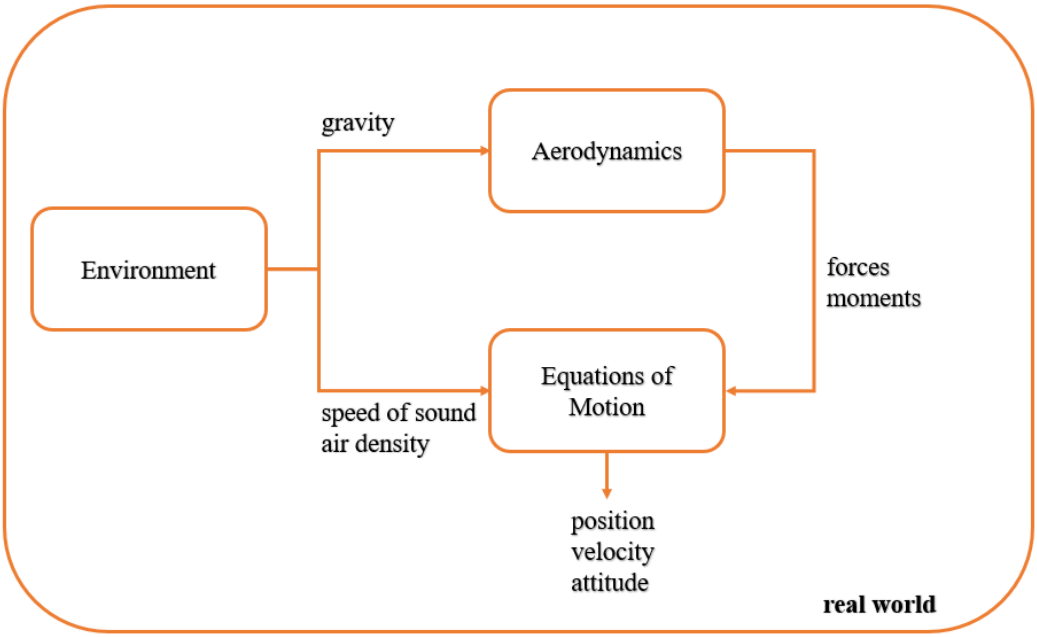

Figure 3-2. Real World Illustration of The Simulation Model

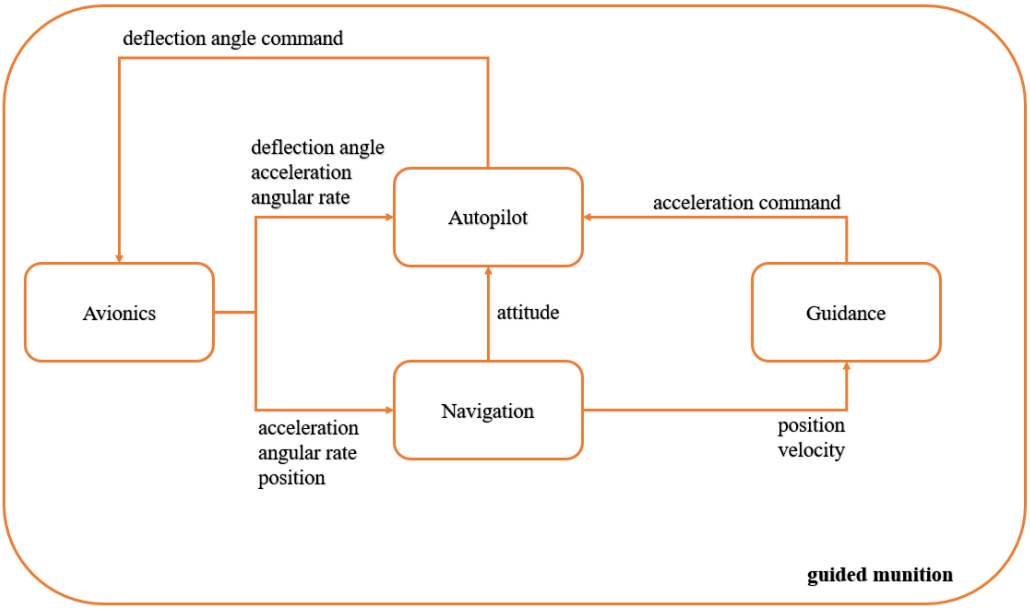

Figure 3-3. Guided Munition Illustration of The Simulation Model

3.1.1 Environment

In the environment section of the simulation model, gravity and atmosphere parameters are modeled. For gravity, the WGS84 Gravity Model (a Matlab-Simulink built-in block) is used. The inputs of this block are the latitude, longitude, and altitude of the guided munition, and the output is the gravity vector in the navigation frame. For the atmosphere, the ISA Atmosphere Model (a Matlab-Simulink built-in block) is used. The input of this block is the altitude of the guided munition, and the outputs are temperature, speed of sound, air pressure, and air density. WGS84 Gravity Model and ISA Atmosphere Model blocks are shown in Figure 3-4.

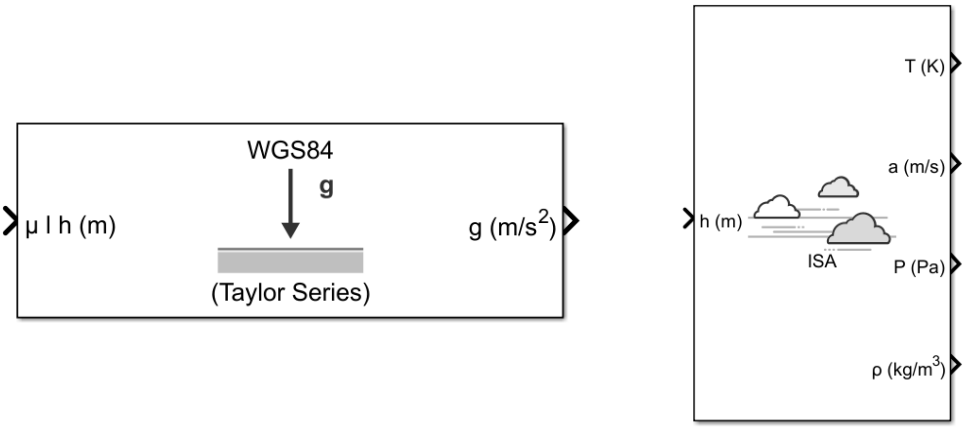

Figure 3-4. Gravity and Atmosphere Blocks From Matlab-Simulink

3.1.2 Aerodynamics

In the aerodynamics section of the simulation model, aerodynamic forces, moments, and parameters are calculated.

3.1.2.1 Forces and Moments

Aerodynamic forces and moments acting on the guided munition's body are illustrated in Figure 3-5.

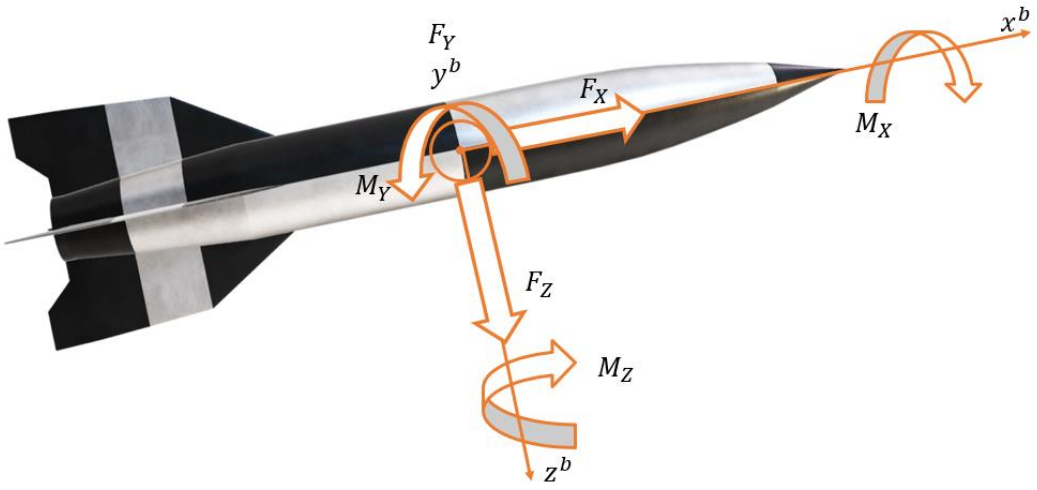

Figure 3-5. Aerodynamic Forces and Moments

Note that aerodynamic forces and moments are represented in Eq. (3.1) and (3.2) to be compatible with the literature.

$$F^b = [F_X \quad F_Y \quad F_Z]^T = [X \quad Y \quad Z]^T \tag{3.1}$$

$$M^b = [M_X \quad M_Y \quad M_Z]^T = [L \quad M \quad N]^T \tag{3.2}$$

Aerodynamic forces and moments are calculated by using static and dynamic aerodynamic coefficients. Aerodynamic coefficients are obtained (by Roketsan) with the Digital Datcom program. Except that C_X and C_Y, aerodynamic coefficients include both static and dynamic parts as stated below. Static coefficients are dependent on the variables given in Table 3.1.

$$C_X = C_{X_{static}} \tag{3.3}$$

$$C_Y = C_{Y_{static}} \tag{3.4}$$

$$C_Z = C_{Z_{static}} + C_{Z_{dynamic}} \tag{3.5}$$

$$C_L = C_{L_{static}} + C_{L_{dynamic}} \tag{3.6}$$

$$C_M = C_{M_{static}} + C_{M_{dynamic}} \tag{3.7}$$

$$C_N = C_{N_{static}} + C_{N_{dynamic}} \tag{3.8}$$

Table 3.1 Static Coefficients and Their Dependent Variables

Static Coefficients	**Dependent Variables**
$C_{X_{static}}$	$M, \alpha, \beta, \delta_e, \delta_r$
$C_{Y_{static}}$	$M, \alpha, \beta, \delta_r$
$C_{Z_{static}}$	$M, \alpha, \beta, \delta_e$
$C_{L_{static}}$	$M, \alpha, \beta, \delta_a$
$C_{M_{static}}$	$M, \alpha, \beta, \delta_e$
$C_{N_{static}}$	$M, \alpha, \beta, \delta_r$

Dynamic coefficients are obtained by using aerodynamic derivatives as given in eq ref. Dynamic derivatives are dependent only on Mach number.

$$C_{Z_{dynamic}} = \frac{C_{z_q} \mathrm{qL_{ref}}}{2V} \tag{3.9}$$

$$C_{L_{dynamic}} = \frac{C_{l_p} \mathrm{pL_{ref}}}{2V} \tag{3.10}$$

$$C_{M_{dynamic}} = \frac{C_{m_q} q L_{ref}}{2V} + \frac{C_{m_{\dot{\alpha}}} \dot{\alpha} L_{ref}}{2V} \tag{3.11}$$

$$C_{N_{dynamic}} = \frac{C_{n_r} r L_{ref}}{2V} + \frac{C_{n_{\dot{\beta}}} \dot{\beta} L_{ref}}{2V} \tag{3.12}$$

Aerodynamic forces and moments are calculated by using aerodynamic coefficients, reference length (L_{ref}), reference area (S_{ref}) ,and dynamic pressure (Q) as in eq

ref. Note that for guided munitions, L_{ref} is the diameter of the body and S_{ref} is the cross-sectional area of the body.

$$X = QS_{ref}C_X \tag{3.13}$$

$$Y = QS_{ref}C_Y \tag{3.14}$$

$$Z = QS_{ref}C_Z \tag{3.15}$$

$$L = QS_{ref}L_{ref}C_L \tag{3.16}$$

$$M = QS_{ref}L_{ref}C_M \tag{3.17}$$

$$N = QS_{ref}L_{ref}C_N \tag{3.18}$$

3.1.2.2 Parameters

In the aerodynamic parameters section of the simulation model, Mach number, angle of attack and sideslip angle is calculated using velocity resolved in the body frame, total velocity, and speed of sound. The angle of attack and sideslip angle are illustrated in Figure 3-6.

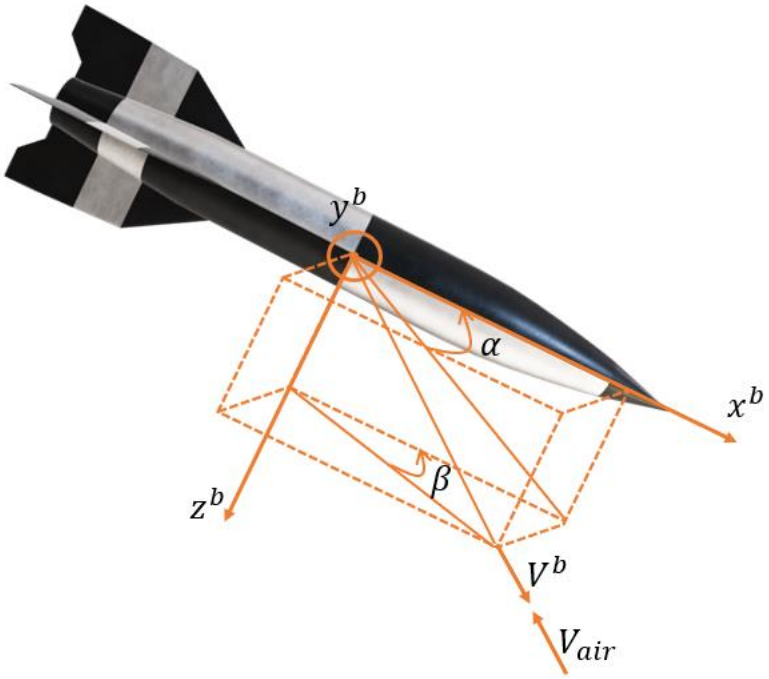

Figure 3-6. Angle of Attack and Sideslip Angle

Angle of attack (α), sideslip angle (β), and Mach number (M) is calculated as in Eq. (3.19), (3.20), and (3.21) [15].

$$\alpha = \text{atan}\frac{w}{u} \tag{3.19}$$

$$\beta = \text{asin}\frac{v}{V} \tag{3.20}$$

$$M = \frac{V}{a} \tag{3.21}$$

Where:

$$V_{eb}^b = [V_x \quad V_y \quad V_z]^T = [u \quad v \quad w]^T \tag{3.22}$$

$$V = \left\| V_{eb}^b \right\| \tag{3.23}$$

3.1.3 Equations of Motion

The equations of motion part of the simulation is divided into two subparts, which are translational and rotational. Both parts include a main differential equation. While the translational part aims to obtain the velocity of the body, the rotational part aims to obtain the angular velocity of the body.

3.1.3.1 Translational

The main differential equation used in this part is given in Eq. (3.24) adapted from [16]. Note that the angular velocities in the equation are calculated in the rotational part.

$$\dot{v}_{eb}^{b} = \frac{F^{b}}{m} + g^{b} - \left(\omega_{ib}^{b} + \omega_{ie}^{b}\right) \times v_{eb}^{b} \tag{3.24}$$

The velocity of the guided munition wrt the Earth is found by integrating the above expression Eq. (3.24). Then, the velocity resolved in the Earth frame is found by multiplying the DCM from the body frame to the Earth frame.

$$V_{eb}^{e} = C_{b}^{e} V_{eb}^{b} \tag{3.25}$$

To calculate latitude(φ), longitude (λ), and altitude (h) of the guided munition, the position vector should be resolved in the Earth frame as in Eq. (3.26)

$$r_{eb}^{e} = \int v_{eb}^{e} \tag{3.26}$$

$$\lambda = \operatorname{atan}\left(\frac{r_{eb}^{e}(2)}{r_{eb}^{e}(1)}\right) \tag{3.27}$$

There are several methods to calculate geodetic latitude. The Bowring Method is used to calculate in this model from [18]. It is an iterative method, and an initial guess of reduced latitude $\left(\bar{\beta}_{0}\right)$ and geodetic latitude (φ_{0}) is needed as given in Eq. (3.28) and (3.29).

$$\bar{\beta}_0 = \operatorname{atan}\left(\frac{r_{eb}^{e}(3)}{(1-f)s}\right) \tag{3.28}$$

$$\varphi_0 = \operatorname{atan}\left(\frac{r_{eb}^{(e)}(3) + \frac{e^2(1-f)}{(1-e^2)} R\left(\sin\bar{\beta}_0\right)^3}{s - e^2 R\left(\cos\bar{\beta}_0\right)^3}\right) \tag{3.29}$$

Where a is equatorial radius of the Earth, e is the square of the first eccentricity, f is the flattening of the Earth, and s is given in Eq. (3.30).

$$s = \sqrt{\left(r_{eb}^{e}(1)\right)^2 + \left(r_{eb}^{e}(2)\right)^2} \tag{3.30}$$

$$a = 6378137.0\ m \tag{3.31}$$

$$f = 0.00335281 \tag{3.32}$$

$$e^2 = 1 - (1-f)^2 \tag{3.33}$$

The reduced latitude $(\bar{\beta})$ is calculated using the Eq. (3.34). Until the geodetic latitude (φ) converges, Eq. (3.34) is repeated.

$$\bar{\beta} = \operatorname{atan}\left(\frac{(1-f)\sin\varphi}{\cos\varphi}\right) \tag{3.34}$$

The altitude (h) is calculated as in Eq. (3.35):

$$h = s\cos\varphi + (r_{eb}^{e}(3) + e^2 R_N \sin\varphi\,)\sin\varphi - R_N \tag{3.35}$$

Where R_N is the normal radius, also known as the radius of curvature of the prime vertical:

$$R_N = \frac{a}{\sqrt{1 - e^2(\sin\varphi)^2}} \tag{3.36}$$

3.1.3.2 Rotational

The main differential equation used in this part is given in Eq. (3.37) [16]:

$$\dot{\omega}_{ib}^{(b)} = [I^b]^{-1}\left(M^b - \omega_{ib}^b I^b \omega_{ib}^b\right) \tag{3.37}$$

Where inertia matrix:

$$I^b = \begin{bmatrix} I_{xx} & -I_{xy} & -I_{zx} \\ -I_{xy} & I_{yy} & -I_{yz} \\ -I_{zx} & -I_{yz} & I_{zz} \end{bmatrix} \tag{3.38}$$

Note that for the guided munition $I_{xy} \approx I_{yz} \approx I_{xz} \approx 0$ because of their symmetry, and inertia matrix becomes:

$$I^b = \begin{bmatrix} I_{xx} & 0 & 0 \\ 0 & I_{yy} & 0 \\ 0 & 0 & I_{zz} \end{bmatrix} \tag{3.39}$$

The direction cosine matrices (DCM) that transform vectors from one reference frame to another reference frame are created under this part of the simulation model. DCM integration method is applied to calculate the DCM as in Eq. (3.40).

$$\dot{C}_b^n = C_b^n skew\left(\omega_{nb}^b\right) \tag{3.40}$$

Where the skew-symmetric matrix of the angular rate of body wrt to the NED-frame:

$$skew\left(\omega_{nb}^b\right) = \begin{bmatrix} 0 & -\omega_{nb}^b(3) & \omega_{nb}^b(2) \\ \omega_{nb}^b(3) & 0 & -\omega_{nb}^b(1) \\ -\omega_{nb}^b(2) & -\omega_{nb}^b(2) & 0 \end{bmatrix} \tag{3.41}$$

$$\omega_{nb}^b = \omega_{ib}^b - C_e^b \omega_{ie}^e - C_n^b \omega_{en}^n \tag{3.42}$$

The angular rate of the navigation frame wrt to Earth frame resolved in the navigation frame is found by Eq. (3.43) [3]:

$$\omega_{en}^n = \begin{bmatrix} \dfrac{V_{eb}^n(2)}{R_N + h} \\ \dfrac{-V_{eb}^n(1)}{R_M + h} \\ \dfrac{V_{eb}^n(2)\tan\varphi}{R_N + h} \end{bmatrix} \tag{3.43}$$

Where the velocity of the body wrt Earth resolved in navigation frame (V_{eb}^{n}), the radius of curvature of the prime vertical (R_M), the angular velocity of the Earth wrt to the inertial frame resolves in Earth frame (ω_{ie}^{e}) are defined in Eq. (3.44), (3.45) and (3.46).

$$V_{eb}^{n} = C_{b}^{n} V_{eb}^{b} \tag{3.44}$$

$$R_M = \frac{a(1-e^2)}{(1-e^2 \sin^2 \mu)^{\frac{3}{2}}} \tag{3.45}$$

$$\omega_{ie}^{e} = \begin{bmatrix} 0 \\ 0 \\ \omega_e \end{bmatrix} \tag{3.46}$$

$$\omega_e = 7.292115 \text{ x } 10^{-5} \frac{\text{rad}}{\text{s}} \tag{3.47}$$

DCM that transforms vectors from Earth frame to the navigation frame is given in Eq. (3.48), which is explained in detail in Chapter 2.2.3. Latitude and longitude of the munition are needed, which is calculated under the translational part of the simulation model.

$$C_{e}^{n} = \begin{bmatrix} -\sin\varphi\cos\lambda & -\sin\varphi\sin\lambda & -\cos\varphi \\ -\sin\lambda & \cos\lambda & 0 \\ -\cos\varphi\cos\lambda & -\cos\varphi\sin\lambda & -\sin\varphi \end{bmatrix} \tag{3.48}$$

Finally, DCM that transforms vectors from the Earth frame to the body frame is found by multiplying two transformation matrices as follows:

$$C_{e}^{b} = C_{n}^{b} C_{e}^{n} \tag{3.50}$$

3.1.4 Avionics

3.1.4.1 Control Actuation System

Control actuation system (CAS) is an electromechanical system that moves the control surfaces of the guided munition according to the commanded autopilot outputs. The control surfaces of the guided munition are tail fins in this study, as stated before in Chapter 2.3. The relationship between the deflection angle command and the deflection angle is modeled as a second-order control system. The Laplace representation of the control system is given in eq ref.

$$\frac{\delta}{\delta_c} = \frac{\omega_{n_{CAS}}^2}{s^2 + 2\zeta_{CAS}\omega_{n_{CAS}}s + \omega_{n_{CAS}}^2} \tag{3.51}$$

3.1.4.2 Inertial Measurement Unit

Three-axis accelerometer and three-axis gyroscope constitute an inertial measurement unit. When accelerometers measure the specific force, gyroscopes measure the rotational velocity of the body with respect to the inertial frame. A tactical grade IMU is chosen for the guided munition. The specifications of the IMU are given in Table 3.2.

Table 3.2 Tactical Grade IMU Specifications

Specifications	**Gyroscope**	**Accelerometer**
Bias Repeatability	$2.5\ °/h$	$0.16\ mg$
Bias Instability	$0.5\ °/h$	$0.1\ mg$
Random Walk	$0.1°/\sqrt{h}$	$0.12\ m/s/\sqrt{h}$
Scale Factor Error	$330\ ppm$	$166\ ppm$

The gyroscope and accelerometer measurements are created in the simulation model given in Eq. (3.52) and (3.53). Bias and noise terms are added to the specific force and angular velocity according to the IMU specifications, which are obtained from the real world part of the simulation. As stated in Chapter 1, specific force is obtained by subtracting the gravity from the acceleration of the body.

$$\tilde{\omega}_{ib}^{b} = \omega_{ib}^{b} + b_g + \varepsilon_g \tag{3.52}$$

$$\tilde{f}_{ib}^{b} = f_{ib}^{b} + b_a + \varepsilon_a \tag{3.53}$$

3.1.4.3 Global Navigation Satellite System Receiver

Global navigation satellite system receiver determines its own position and velocity by using signals from the satellites which contain information of the satellites' position, velocity, and time. Several satellites' position and velocity data are created by using two-line element data set. More information regarding this can be found in [19]. By using satellites' position and velocity data, pseudo-range and pseudo-range rate measurements are created as in Eq. (3.54) and (3.56) [3].

$$\rho_{GNSS}^{m} = r^{m} + b_{GNSS}^{m} + \tilde{\varepsilon}_{\rho}^{m} \tag{3.54}$$

Where the range between the satellite and the receiver is r^m and line of sight unit vector 1_{LOS}^{m} is defined as:

$$r^{m} = \|(r_{eb}^{e} - r_{GNSS}^{m})\| \tag{3.55}$$

$$1_{LOS}^{m} = \frac{(r_{eb}^{e} - r_{GNSS}^{m})}{r^{m}} \tag{3.56}$$

$$\dot{\rho}_{GNSS}^{m} = (v_{GNSS}^{m} - v_{eb}^{e}).1_{LOS}^{m} + d_{GNSS}^{m} + \tilde{\varepsilon}_{\dot{\rho}}^{m} \tag{3.56}$$

Pseudo-range and pseudo-range rate measurements can be used directly in tightly coupled INS/GNSS integration. For loosely coupled INS/GNSS integration, position and velocity estimation from the GNSS receiver is necessary and found by using the

least squares algorithm. More information regarding this can be found in Appendix A.

3.1.5 Navigation

In the navigation section of the simulation model, the position, velocity, and attitude of the guided munition are calculated by using IMU measurements and/or INS/GPS integration. IMU measurements are used in the equations given in Chapter 3.1.3. The only difference is that instead of using aerodynamic forces and moments, specific force and angular velocity measurements from the IMU are utilized. INS/GPS integration is achieved with both loosely coupled and tightly coupled integration methods. For both methods, the error-state Kalman filter is utilized. INS/GPS integration is explained in detail in Chapter 3.2.

3.1.6 Autopilot

Autopilots are designed for pitch, yaw, and roll dynamics separately. Full state-feedback autopilots are designed, and with the purpose of decreasing the steady state error, an integral is added to the system. While the aim of pitch and yaw autopilots is achieving the commanded acceleration from the guidance, roll autopilot tries to keep the body roll angle (ϕ) at zero. During the design of the autopilots, aerodynamic derivatives are obtained from the aerodynamic database, and linear matrices belonging to the three separate dynamics of the guided munition are created using equations of motion. The derivation of the linear matrices is given in Appendix B. Control system model with linear matrices (A, B, C, D) is given in Eq. (3.57) and (3.58).

$$\dot{x} = Ax + Bu \tag{3.57}$$

$$y = Cx + Du \tag{3.58}$$

The state-space control system with an integrator structure is given in Figure 3-7 [20].

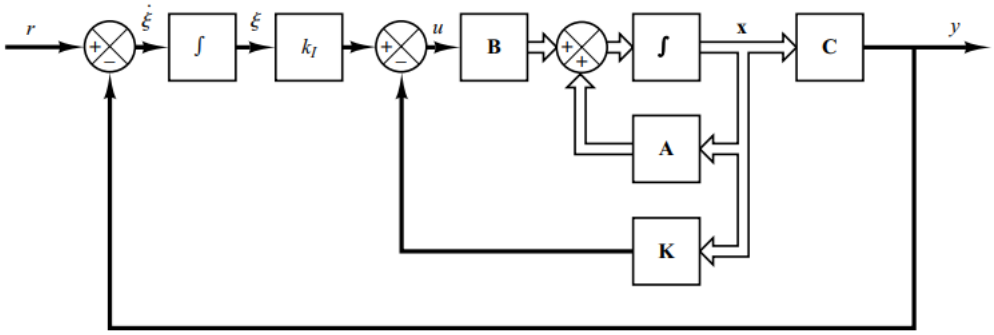

Figure 3-7. State-Space Control System with An Integrator [20]

The linear system matrices for pitch dynamics are given in Eq. (3.59) and (3.60):

$$\begin{bmatrix} \dot{a_Z} \\ \dot{q} \\ \dot{\delta} \\ \ddot{\delta} \end{bmatrix} = \begin{bmatrix} \frac{Z_\alpha}{mu} + \frac{Z_q M_\alpha}{Z_\alpha I_y} & \frac{Z_\alpha}{m} + \frac{Z_q M_q}{m I_y} - \frac{Z_q^2 M_\alpha}{Z_\alpha m I_y} & -\frac{Z_q M_\alpha Z_\delta}{Z_\alpha m I_y} + \frac{Z_q M_\delta}{m I_y} & \frac{Z_\delta}{m} \\ \frac{M_\alpha m}{I_y Z_\alpha} & \frac{M_q}{I_y} - \frac{M_\alpha Z_q}{Z_\alpha I_y} & \frac{M_\delta}{I_y} - \frac{M_\alpha Z_\delta}{Z_\alpha I_y} & 0 \\ 0 & 0 & 0 & 1 \\ 0 & 0 & -\omega_n^2 & -2\zeta\omega_n^2 \end{bmatrix} \begin{bmatrix} a_Z \\ q \\ \delta \\ \dot{\delta} \end{bmatrix} + \begin{bmatrix} 0 \\ 0 \\ 0 \\ \omega_n^2 \end{bmatrix} \delta_c \quad (3.59)$$

$$a_Z = \begin{bmatrix} 1 & 0 & 0 & 0 \end{bmatrix} \begin{bmatrix} a_Z \\ q \\ \delta \\ \dot{\delta} \end{bmatrix} \quad (3.60)$$

The linear system matrices for yaw dynamics are given in Eq. (3.61) and (3.62):

$$\begin{bmatrix} \dot{a_Y} \\ \dot{r} \\ \dot{\delta} \\ \ddot{\delta} \end{bmatrix} = \begin{bmatrix} \frac{Y_\beta}{mV} + \frac{Y_r N_\beta}{Y_\beta I_z} & -\frac{Y_\beta}{m} + \frac{Y_r N_r}{mI_z} - \frac{Y_r^2 N_\beta}{Y_\beta m I_z} & -\frac{Y_r N_\beta Y_\delta}{Y_\beta m I_z} + \frac{Y_r N_\delta}{mI_z} & \frac{Y_\delta}{m} \\ \frac{N_\beta m}{Y_\beta I_z} & \frac{N_r}{I_z} - \frac{N_\beta Y_r}{Y_\beta I_z} & \frac{N_\delta}{I_z} - \frac{N_\beta Y_\delta}{Y_\beta I_z} & 0 \\ 0 & 0 & 0 & 1 \\ 0 & 0 & -\omega_n^2 & -2\zeta\omega_n^2 \end{bmatrix} \begin{bmatrix} a_Y \\ r \\ \delta \\ \dot{\delta} \end{bmatrix} + \begin{bmatrix} 0 \\ 0 \\ 0 \\ \omega_n^2 \end{bmatrix} \delta_c \tag{3.61}$$

$$a_Y = \begin{bmatrix} 1 & 0 & 0 & 0 \end{bmatrix} \begin{bmatrix} a_Y \\ q \\ \delta \\ \dot{\delta} \end{bmatrix} \tag{3.62}$$

The linear system matrices for roll dynamics are given in Eq. (3.63) and (3.64):

$$\begin{bmatrix} \dot{\phi} \\ \dot{p} \\ \dot{\delta} \\ \ddot{\delta} \end{bmatrix} = \begin{bmatrix} 0 & 1 & 0 & 0 \\ 0 & \frac{L_p}{I_x} & \frac{L_\delta}{I_x} & 0 \\ 0 & 0 & 0 & 1 \\ 0 & 0 & -\omega_n^2 & -2\zeta\omega_n^2 \end{bmatrix} \begin{bmatrix} \phi \\ p \\ \delta \\ \dot{\delta} \end{bmatrix} + \begin{bmatrix} 0 \\ 0 \\ 0 \\ \omega_n^2 \end{bmatrix} \delta_c \tag{3.63}$$

$$\phi = \begin{bmatrix} 1 & 0 & 0 & 0 \end{bmatrix} \begin{bmatrix} \phi \\ p \\ \delta \\ \dot{\delta} \end{bmatrix} \tag{3.64}$$

3.1.7 Guidance

The proportional navigation guidance law is applied in this study. This law states that if the interceptor closes to the target such that the line-of-sight vector does not rotate with respect to the initial reference frame then the interceptor can have a successful collision with the target [21]. In other words, the interceptor should have acceleration such that the angular rate of the line-of-sight vector is equal to zero. A guidance schematic is given in Figure 3-8.

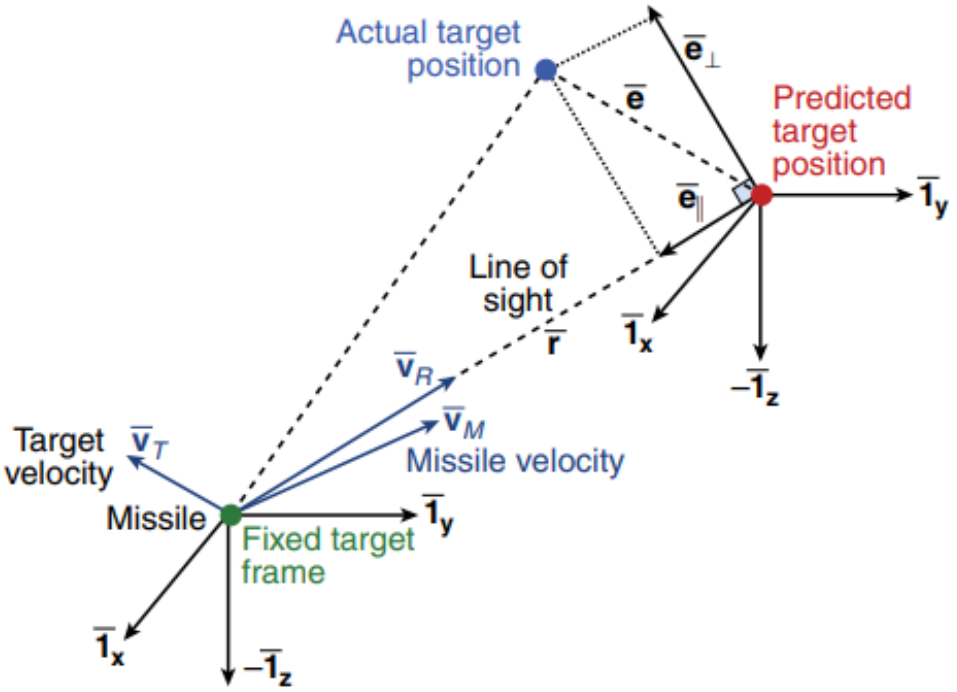

Figure 3-8. Guidance Schematic [21]

The line-of-sight angular rate is calculated as in Eq. (3.65).

$$\omega_{LOS} = \frac{r_{bt}^n \times V_{bt}^n}{\|r_{bt}\|^2} \tag{3.65}$$

The acceleration command is calculated as in Eq. (3.66):

$$a_{com}^n = N_{PNG}\omega_{LOS} \times V_{eb}^n \tag{3.66}$$

$$a_{com}^b = C_n^b a_{com}^n \tag{3.67}$$

3.2 INS/GPS Integration

In this study, both loosely coupled and tightly coupled approaches are applied for the INS/GPS integration. Error-state Kalman filter is utilized for both approaches. These integration methods differ in system models and measurement models, that are explained in Chapter 3.2.1.2 and 3.2.2.2.

3.2.1 Loosely Coupled Integration

In loosely coupled integration, both INS and GNSS provide separate position and velocity solutions, and then, with the help of error-state Kalman solutions from both sensors are combined to have better navigation solutions. A schematic from [3] is given in Figure 3-9.

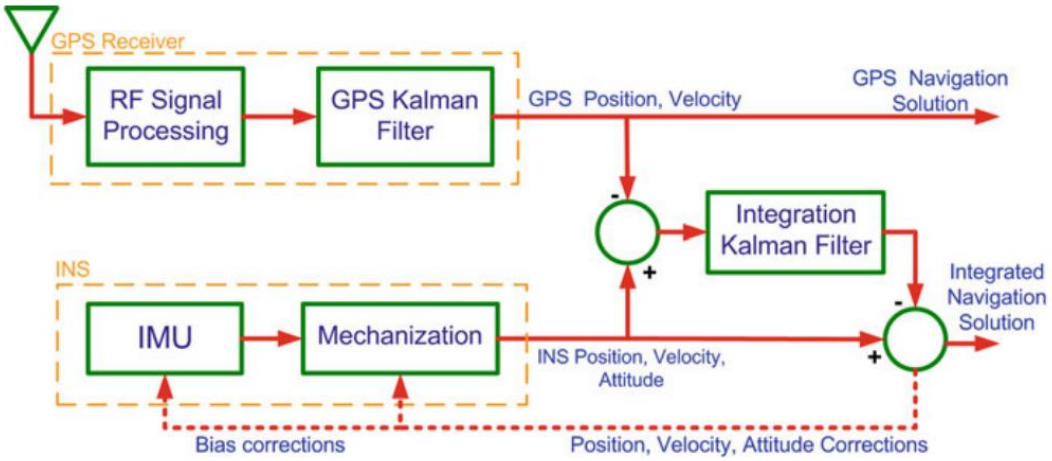

Figure 3-9. Loosely Coupled INS/GNSS integration [3]

3.2.1.1 System Model

The continuous system model of the error state Kalman filter for loosely coupled architecture is given below [22]. Where δ_x is the error-state vector, F is the dynamic coefficient matrix, u is the forcing vector, and B is the design matrix.

$$\delta\dot{x} = F\delta x + Bu \tag{3.68}$$

Where the vectors are defined as:

$$\delta x = [\delta r \quad \delta v^n \quad \delta\alpha]^T \tag{3.69}$$

$$\delta r = [\delta\varphi \quad \delta\lambda \quad \delta h]^T \tag{3.70}$$

$$\delta v^n = [\delta v_N \quad \delta v_E \quad \delta v_D]^T \tag{3.71}$$

$$\delta\alpha = [\delta\phi \quad \delta\theta \quad \delta\psi]^T \tag{3.72}$$

$$u = [\delta f_{ib}^b \quad \delta\omega_{ib}^b] \tag{3.73}$$

$$\delta f_{ib}^b = [b_a \quad b_a \quad b_a]^T \tag{3.74}$$

$$\delta\omega_{ib}^b = [b_g \quad b_g \quad b_g]^T \tag{3.75}$$

The dynamic coefficient matrix and design matrix are illustrated in Eq. (3.76) and (3.77).

$$F = \begin{bmatrix} F_{rr} & F_{rv} & 0_{3x3} \\ F_{vr} & F_{vv} & skew(f_{ib}^n) \\ F_{\alpha r} & F_{\alpha v} & -skew(\omega_{in}^n) \end{bmatrix} \tag{3.76}$$

$$B = \begin{bmatrix} 0_{3x3} & 0_{3x3} \\ C_b^n & 0_{3x3} \\ 0_{3x3} & -C_b^n \end{bmatrix} \tag{3.77}$$

The elements of the dynamic coefficient matrix for the position part (F_{rr}, F_{rv}) are given in Eq. (3.78) and (3.79).

$$F_{rr} = \begin{bmatrix} 0 & 0 & -\dfrac{v_N}{(R_M + h)^2} \\ \dfrac{v_E \sin\varphi}{(R_N + h)} & 0 & -\dfrac{v_E}{(R_N + h)^2 \cos\varphi} \\ 0 & 0 & 0 \end{bmatrix} \tag{3.78}$$

$$F_{rv} = \begin{bmatrix} \dfrac{1}{R_M + h} & 0 & 0 \\ 0 & \dfrac{1}{(R_N + h)\cos\varphi} & 0 \\ 0 & 0 & -1 \end{bmatrix} \tag{3.79}$$

The elements of the dynamic coefficient matrix for the velocity part (F_{vr}, F_{vv}) given below.

$$F_{vr} = \begin{bmatrix} -2v_E\omega_e \cos\varphi - \dfrac{v_E^2}{(R_N+h)\cos^2\varphi} & 0 & -\dfrac{v_N v_D}{(R_M+h)^2} + \dfrac{v_E^2 \tan\varphi}{(R_N+h)^2} \\ 2\omega_e(v_N \cos\varphi - v_D \sin\varphi) & 0 & -\dfrac{v_E v_D}{(R_N+h)^2} - \dfrac{v_N v_E \tan\varphi}{(R_N+h)^2} \\ 2v_E\omega_e \sin\varphi & 0 & \dfrac{v_E^2}{(R_N+h)^2} + \dfrac{v_N^2}{(R_M+h)^2} - \dfrac{2\gamma}{(R+h)} \end{bmatrix} \quad (3.80)$$

$$F_{vv} = \begin{bmatrix} \dfrac{v_D}{R_M+h} & -2\omega_e \sin\varphi - \dfrac{2v_E \tan\varphi}{R_N+h} & \dfrac{v_N}{R_M+h} \\ 2\omega_e \sin\varphi + \dfrac{v_E \tan\varphi}{R_N+h} & \dfrac{v_D + v_N \tan\varphi}{R_N+h} & 2\omega_e \cos\varphi + \dfrac{v_E}{R_N+h} \\ -\dfrac{2v_N}{R_M+h} & -2\omega_e \cos\varphi - \dfrac{2v_E}{R_N+h} & 0 \end{bmatrix} \quad (3.81)$$

$$skew(f_{ib}^n) = \begin{bmatrix} 0 & -f_D & f_E \\ f_D & 0 & -f_N \\ -f_E & f_N & 0 \end{bmatrix} \quad (3.82)$$

The elements of the dynamic coefficient matrix for the attitude part $(F_{\alpha r}, F_{\alpha v})$ given below.

$$F_{\alpha r} = \begin{bmatrix} -\omega_e \sin\varphi & 0 & -\dfrac{v_E}{(R_N+h)^2} \\ 0 & 0 & \dfrac{v_N}{(R_M+h)^2} \\ -\omega_e \cos\varphi - \dfrac{v_E}{(R_N+h)\cos^2\varphi} & 0 & \dfrac{v_E \tan\varphi}{(R_N+h)^2} \end{bmatrix} \quad (3.83)$$

$$F_{\alpha v} = \begin{bmatrix} 0 & \dfrac{1}{R_N+h} & 0 \\ \dfrac{-1}{R_M+h} & 0 & 0 \\ 0 & \dfrac{-\tan\varphi}{R_N+h} & 0 \end{bmatrix} \quad (3.84)$$

By utilizing the continuous system model, the discrete system model of the error-state Kalman filter for loosely coupled integration is found as below.

$$\delta x_{k+1} = (I_{9x9} + F\Delta t)\delta x_k + w_k \quad (3.85)$$

Where:

$$E[w_k w_i^T] = \begin{cases} Q_k & i = k \\ 0 & i \neq k \end{cases} \tag{3.86}$$

3.2.1.2 Measurement Model

The measurement model of the error-state Kalman filter for loosely coupled INS/GPS integration is given in discrete form [22].

$$\delta z_k = H_k \delta x_k + e_k \tag{3.87}$$

Where:

$$\delta z_k = \begin{bmatrix} r_{INS}^n - r_{GPS}^n \\ v_{INS}^n - v_{GPS}^n \end{bmatrix} \tag{3.88}$$

$$H_k = \begin{bmatrix} I_{3x3} & 0_{3x3} & 0_{3x3} \\ 0_{3x3} & I_{3x3} & 0_{3x3} \end{bmatrix} \tag{3.89}$$

$$E[e_k e_i^T] = \begin{cases} R_k & i = k \\ 0 & i \neq k \end{cases} \tag{3.90}$$

$$E[w_k e_i^T] = 0 \qquad \forall i, k \tag{3.91}$$

3.2.2 Tightly Coupled Integration

In tightly coupled integration, GNSS measures pseudo-range and pseudo-range rates, and by using INS navigation solutions, pseudo-range and pseudo-range rate measurements are imitated. Both measurements are used in an error state Kalman filter. Tightly coupled INS/GNSS integration is illustrated in Figure 3-10 from [3].

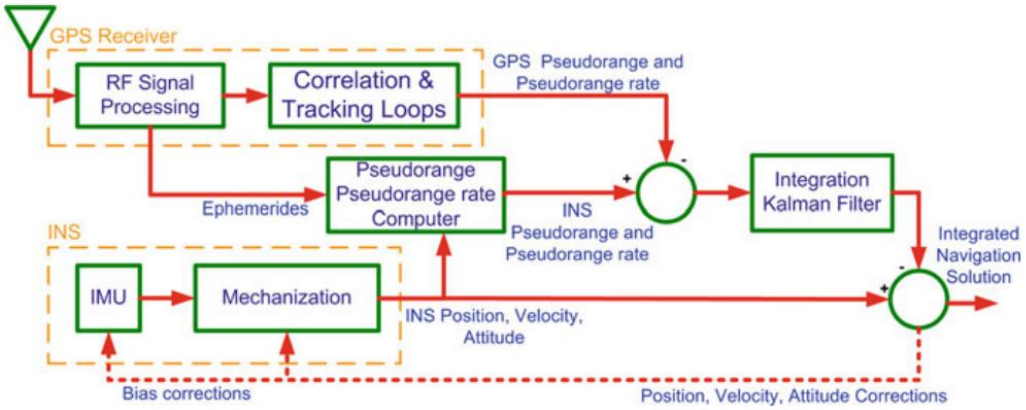

Figure 3-10. Tightly Coupled INS/GNSS Integration [3]

3.2.2.1 System Model

For the system model of the tightly coupled integration, states related to the GPS measurements are added to the system matrix and state vector. GNSS states include GPS clock bias and drift. The time derivative of the GPS measurement bias is modeled as the drift. The other parts are the same as the loosely coupled system, which can be found in detail in Chapter 3.2.1.1. The system model for the GNSS part is given as [3] in Eq. (3.92):

$$\delta \dot{x}_G = F_G \delta x_G + G_G w_G \tag{3.92}$$

Where:

$$\delta x = [\delta b_G \quad \delta d_G]^T \tag{3.93}$$

$$F_G = \begin{bmatrix} 0 & 1 \\ 0 & 0 \end{bmatrix} \tag{3.94}$$

$$G_G = [\sigma_b \quad \sigma_d]^T \tag{3.95}$$

Together with the loosely coupled system matrix:

$$F = \begin{bmatrix} F_{LC} & 0 \\ 0 & F_G \end{bmatrix} \tag{3.96}$$

3.2.2.2 Measurement Model

The measurement model of the error-state Kalman filter for tightly coupled INS/GNSS integration is given in discrete form. While the loosely coupled measurement model considers the position and velocity differences from INS and GPS as measurements, the tightly coupled measurement model considers pseudo-range and pseudo-range rate differences from INS and GNSS. For this purpose, pseudo-range and pseudo-range rate measurements are imitated by using INS measurements, as shown in Eq. (3.104) and (3.106).

$$\delta z_k = H_k \delta x_k + \mathrm{e_k} \tag{3.97}$$

Where:

$$H_k = \begin{bmatrix} H^{\rho}_{Mx3} & 0_{Mx3} & 0_{Mx3} & -ones(M,1) & 0_{Mx1} \\ 0_{Mx3} & H^{\dot{\rho}}_{Mx3} & 0_{Mx3} & 0_{Mx1} & -ones(M,1) \end{bmatrix} \tag{3.98}$$

$$H^{\rho} = G_{Mx3} T_{3x3} \tag{3.99}$$

$$G = \begin{bmatrix} (1^1_{LOS})^T \\ (1^2_{LOS})^T \\ \vdots \\ (1^M_{LOS})^T \end{bmatrix} \tag{3.100}$$

$$T = \begin{bmatrix} -(R_N + h)\sin\varphi\cos\lambda & -(R_N + h)\cos\varphi\sin\lambda & \cos\varphi cos\lambda \\ -(R_N + h)\sin\varphi\sin\lambda & (R_N + h)\cos\varphi\cos\lambda & cos\varphi\sin\lambda \\ \{R_N(1 - e^2) + h\}\cos\varphi & 0 & \sin\varphi \end{bmatrix} \tag{3.101}$$

$$H^{\dot{\rho}} = G_{Mx3} C^e_n \tag{3.102}$$

$$\delta z_k = \begin{bmatrix} \delta z_{\rho} \\ \delta z_{\dot{\rho}} \end{bmatrix} = \begin{bmatrix} \rho^1_{INS} - \rho^1_{GNSS} \\ \vdots \\ \rho^M_{INS} - \rho^M_{GNSS} \\ \dot{\rho}^1_{INS} - \dot{\rho}^1_{GNSS} \\ \vdots \\ \dot{\rho}^M_{INS} - \dot{\rho}^M_{GNSS} \end{bmatrix} \tag{3.103}$$

Where:

$$\rho_{INS}^{m} = \left\| \left(r_{eb,INS}^{e} - r_{GNSS}^{m} \right) \right\| \tag{3.104}$$

$$1_{LOS,INS}^{m} = \frac{\left(r_{eb,INS}^{e} - r_{GNSS}^{m} \right)}{\left\| \left(r_{eb,INS}^{e} - r_{GNSS}^{m} \right) \right\|} \tag{3.105}$$

$$\dot{\rho}_{INS}^{m} = \left(v_{eb,INS}^{m} - v_{GNSS}^{m} \right). 1_{LOS,INS}^{m} \tag{3.106}$$

3.3 Error-State Kalman Filter

For the error-state Kalman filter, system and measurement models are provided in Chapters 3.2.1 and 3.2.2. To implement the Kalman filter, time update and measurement update equations are necessary.

3.3.1 Time Update

$$\delta \hat{x}^{-} = (I + F_k \Delta t) \delta \hat{x}_{k-1} \tag{3.107}$$

$$P_{k+1}^{-} = (I + F_k \Delta t) P_k (I + F_k \Delta t)^T + Q_k \tag{3.108}$$

3.3.2 Measurement Update

$$K_k = P_k^{-} H_k^T \left(H_k P_k^{-} H_k^T + R_k \right)^{-1} \tag{3.109}$$

$$\delta \hat{x}_k = \delta \hat{x}_k^{-} + K_k (\delta z_k - H_k \delta \hat{x}_k^{-}) \tag{3.110}$$

$$P_k = (I - K_k H_k) P_k^{-} \tag{3.111}$$

3.4 Adaptive Kalman Filter

Adaptive Kalman filtering is achieved by innovation-based R-adaptation by both single-scale factor (SSF) and multiple-scale factor (MSF) from [13]. The faulty measurement can be detected with the help of a statistical function, β_k [13]. Without the faulty measurement, the statistical function must follow the square of normal

distribution and have a value lower than a defined threshold. In case of a faulty measurement, β_k value increases significantly. When β_k is higher than a specific value found from chi-square table, then the measurement noise covariance matrix (R_k) could be adapted by using SSF and MSF approaches [14]. The calculation of the statistical function (β_k) involves residual, which is a measure of the difference between measurement and the estimated value.

$$\beta_k = \tilde{e}_k^T \left(H_k P_{k|k-1} H_k^T + R_k\right)^{-1} \tilde{e}_k \tag{3.112}$$

Where the residual is defined as in Eq. (3.113):

$$\tilde{e}_k = y_k - H_k \hat{x}_{k|k-1} \tag{3.113}$$

3.4.1 Single Scale Factor

Single scale factor is calculated as in Eq. (3.114) and the resultant is a scalar which is multiplied with the measurement noise covariance matrix (R_k) as in Eq. (3.115).

$$S_k = \frac{\tilde{e}_k{}^T \tilde{e}_k - tr\{H_k P_{k|k-1} H_k^T\}}{tr\{R_k\}} \tag{3.114}$$

$$R_k = S_k R_k \tag{3.115}$$

3.4.2 Multiple Scale Factor

Multiple scale factor is calculated as in Eq. (3.114) and the resultant is a scalar which is multiplied with the measurement noise covariance matrix (R_k) as in Eq. (3.115). MSF could be beneficial in case some of the measurements are faulty; some valuable measurements are unwanted to be lost.

$$S_k = \left(\tilde{e}_k{}^T \tilde{e}_k - H_k P_{k|k-1} H_k^T\right) R_k^{-1} \tag{3.116}$$

$$R_k = S_k R_k \tag{3.117}$$

However, MSF matrix, S_k, sometimes can be non-diagonal or have values less than 1 which decreases some values of the measurement noise covariance matrix [14]. Both cases are undesired and need to be fixed. For this purpose, a rule is defined as in Eq. (3.118) [14]:

$$S_k^* = diag(s_1^* \quad s_2^* \quad \cdots \quad s_n^*) \tag{3.118}$$

Where:

$$s_i^* = \max\{1, S_{ii}\} \tag{3.119}$$

CHAPTER 4

RESULTS AND DISCUSSION

4.1 The Guided Munition Scenario

Navigation results are obtained by using the simulation model. Errors are created by calculating the difference between the real world and KF navigation results. In the scenario studied, the guided munition is released from a host vehicle from 6000 m to the target in 10 km downrange and 500 m cross range, as can be observed from Figure 4-1.

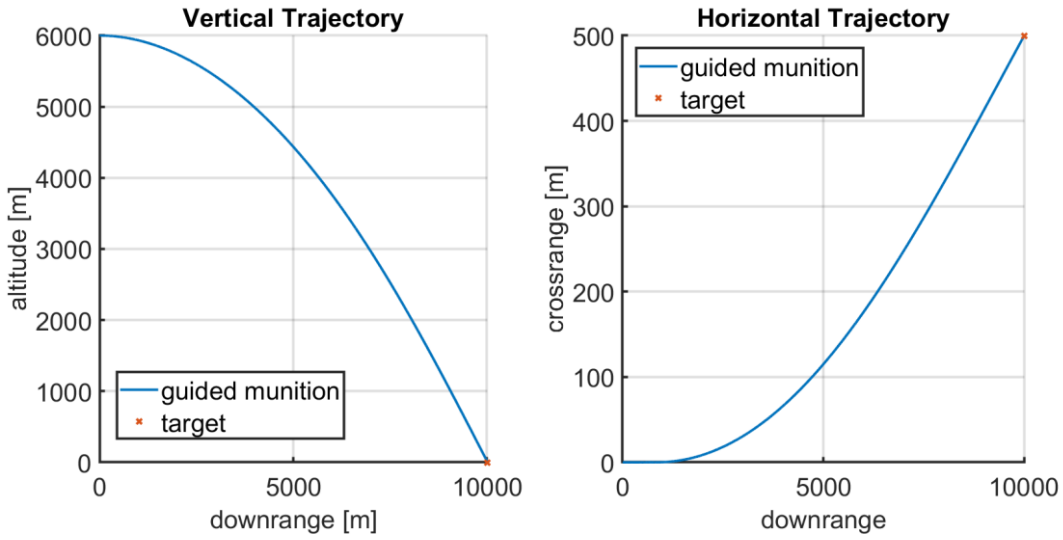

Figure 4-1 Flight Trajectories

In Figure 4-2, the Mach number, angle of attack, and side slip angle of the guided munition are presented. The guided munition is released with a Mach number of 0.85 and it has positive angle of attack during flight.

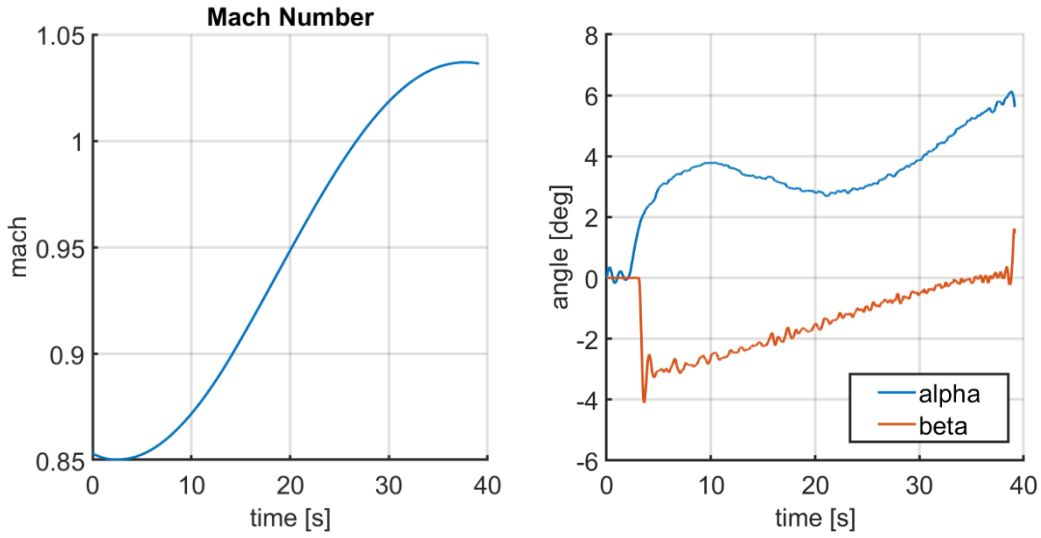

Figure 4-2 Mach Number, Angle of Attack and Sideslip Angle

In Figure 4-3, Euler angles and body angular rates are illustrated. As expected, the body roll angle is zero during flight, thanks to the roll autopilot. Pitch and yaw angles are the natural outcome of the scenario and guidance law.

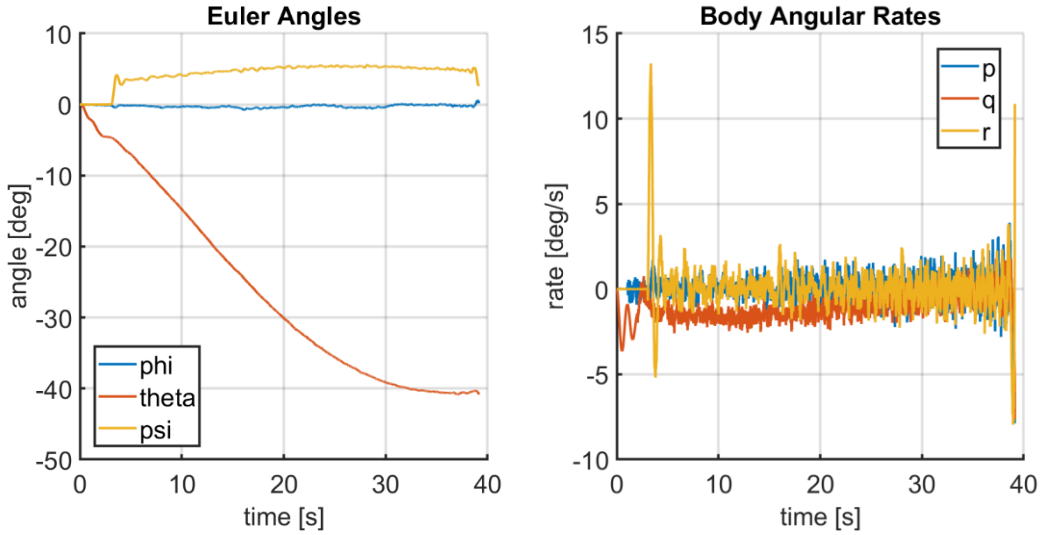

Figure 4-3 Euler Angles and Angular Rates

Acceleration commands and responses for pitch and yaw channels are illustrated in Figure 4-4. Both autopilots successfully follow the acceleration commands as observed.

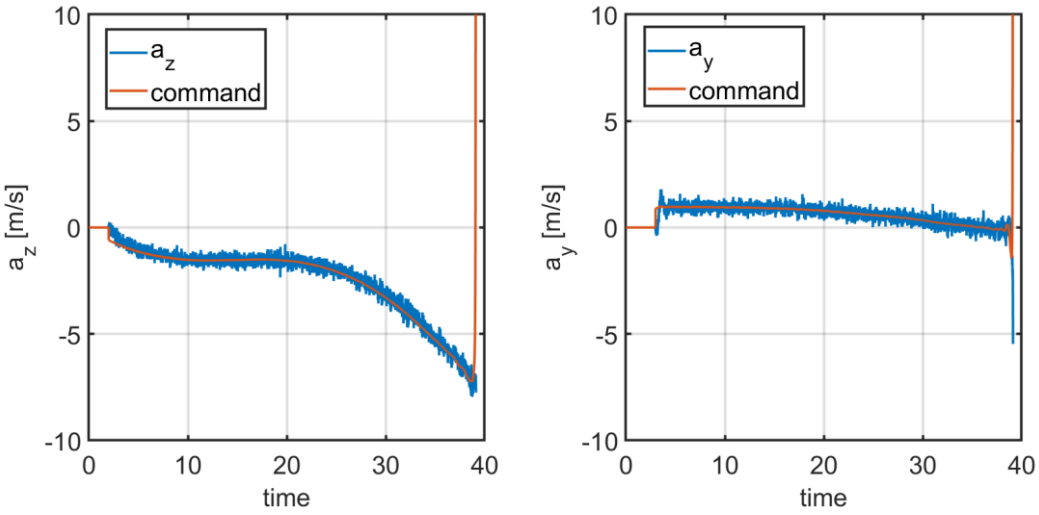

Figure 4-4 Acceleration Commands and Responses

4.2 Navigation Errors with Loosely Coupled Integration

Navigation errors for position, velocity, and attitude are provided in Figure 4-5, Figure 4-6, and Figure 4-7. Except for the second Euler angle, all of the errors stay in the theoretical 3σ bounds when no GPS measurement faults are present.

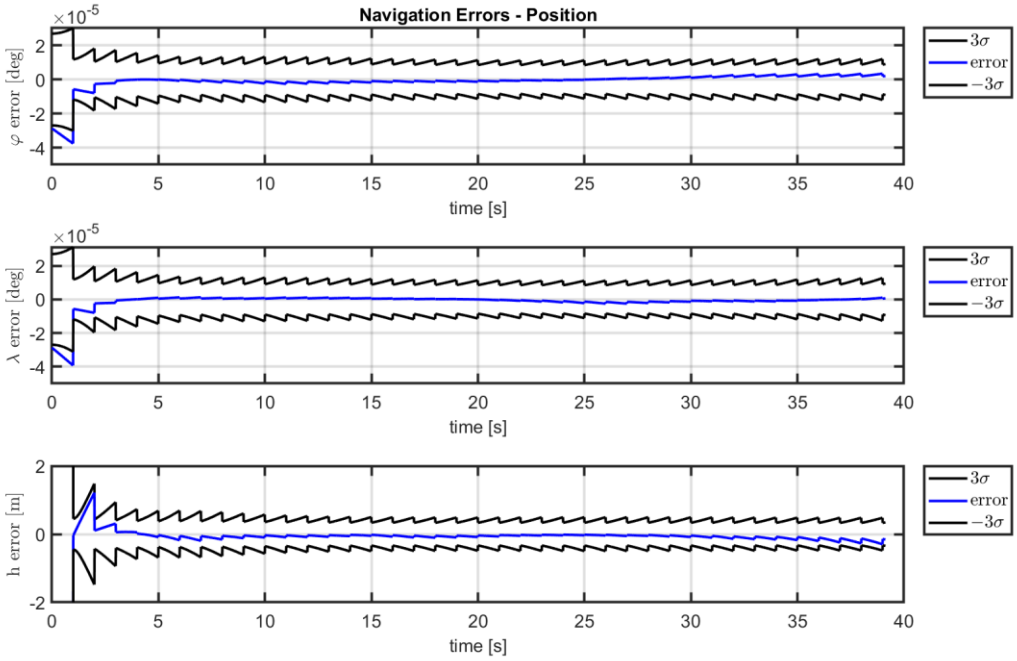

Figure 4-5 Loosely Coupled Integration Position Errors

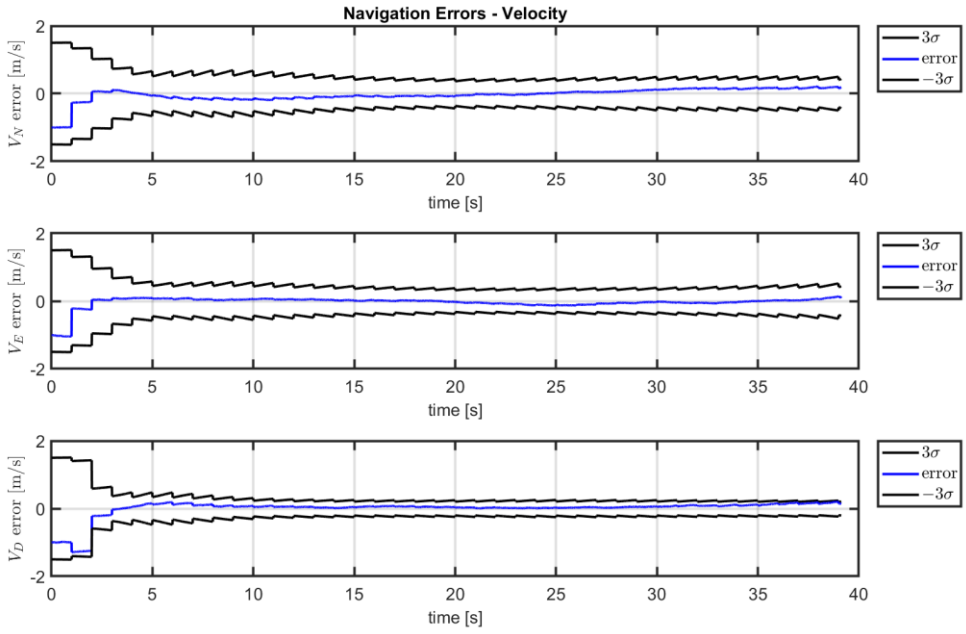

Figure 4-6 Loosely Coupled Integration Velocity Errors

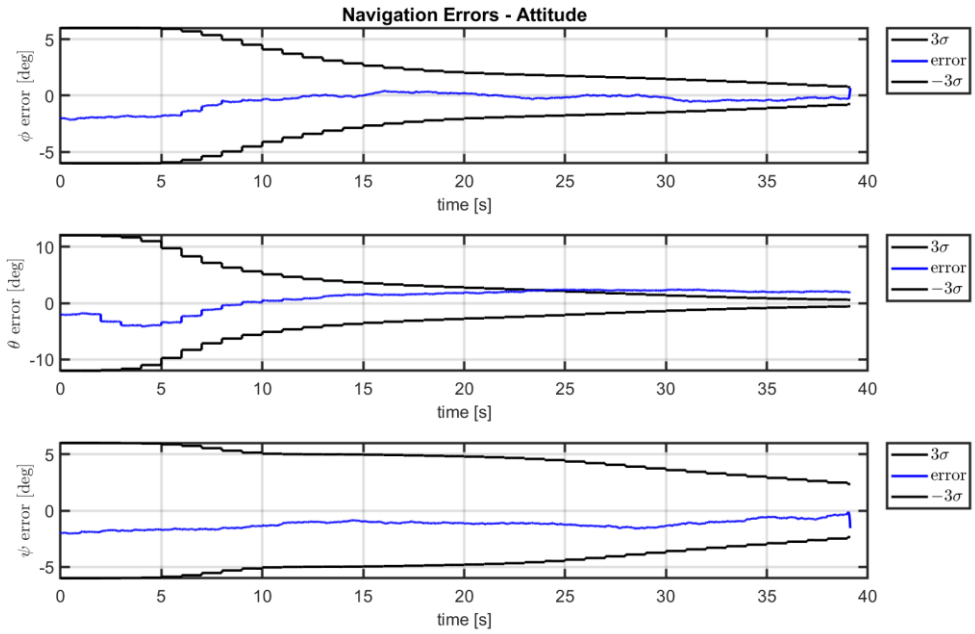

Figure 4-7 Loosely Coupled Integration Attitude Errors

4.3 Navigation Errors with Tightly Coupled Integration

For tightly coupled integration, navigation errors of position, velocity, and attitude are provided in Figure 4-8, Figure 4-9, and Figure 4-10. Every error stays in the theoretical 3σ bounds when no GPS measurement faults are present.

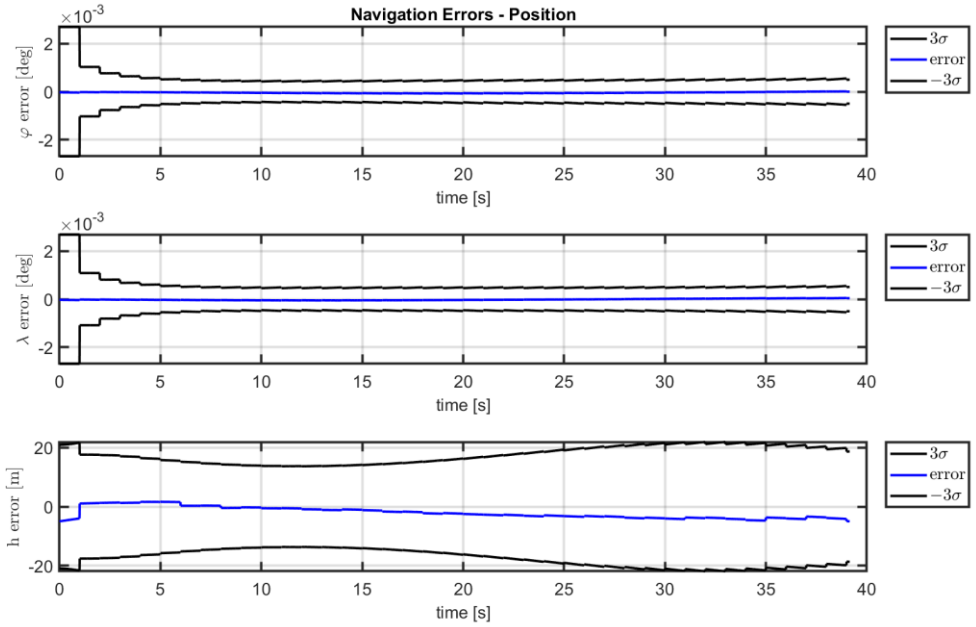

Figure 4-8 Tightly Coupled Integration Position Errors

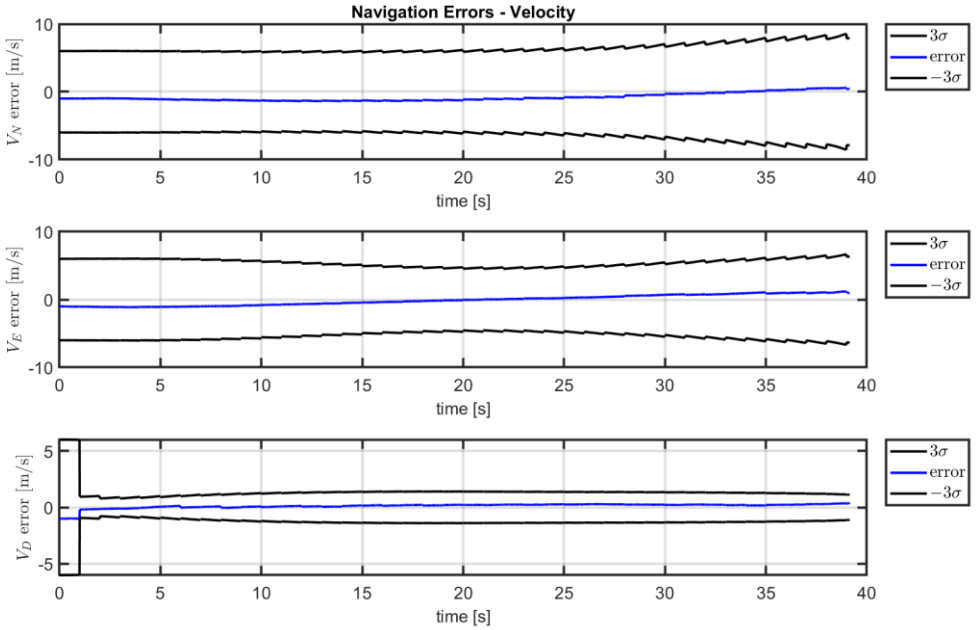

Figure 4-9 Tightly Coupled Integration Velocity Errors

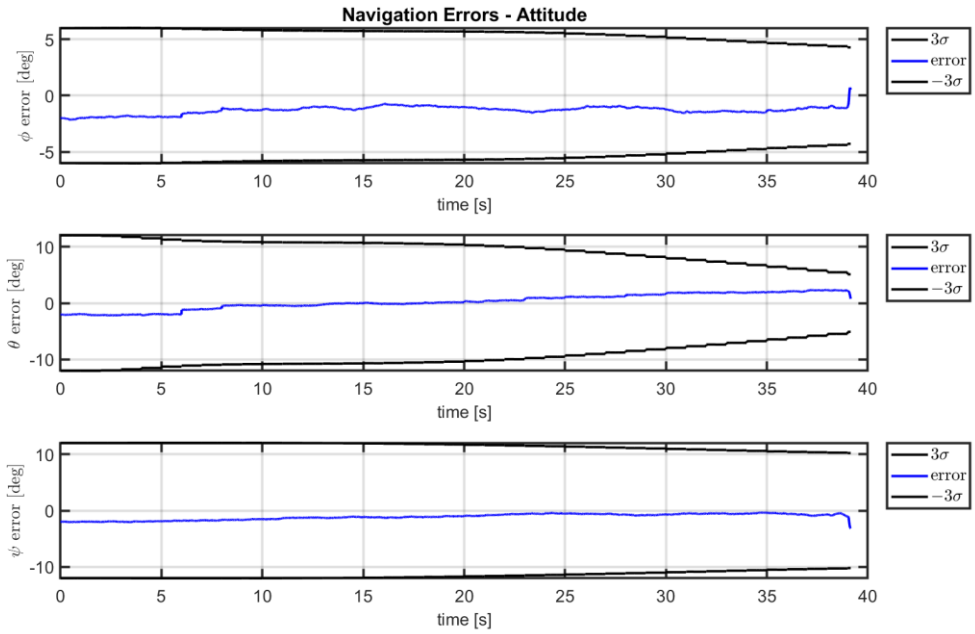

Figure 4-10 Tightly Coupled Integration Attitude Errors

4.4 Navigation Errors Under GNSS Spoofing

To create a GNSS spoofing error case, one of the measurements from the GPS is disrupted at the 20th second by adding some bias for 5 seconds. The goal was to compare the navigation errors for both loosely coupled and tightly coupled integration methods in case of faulty measurements and then observe the improvement with the adaptive KF if there are any. However, for the same error comparison, the least squares algorithm, which is utilized in loosely coupled integration methods to obtain the guided munition's position and velocity using pseudo-range and pseudo-range rate measurements, cannot provide any reasonable solutions in the case of faulty measurements. The guided munition position and bias solution found by the least squares algorithm is provided in Figure 4-11 and Figure 4-12. As soon as GPS pseudo-range and pseudo-range rate errors are introduced, the position and bias solution increases excessively.

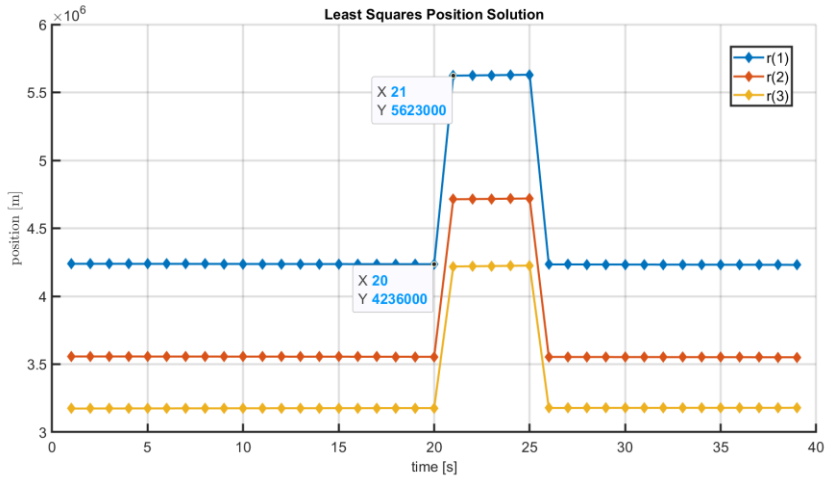

Figure 4-11 Least Squares Position Solution

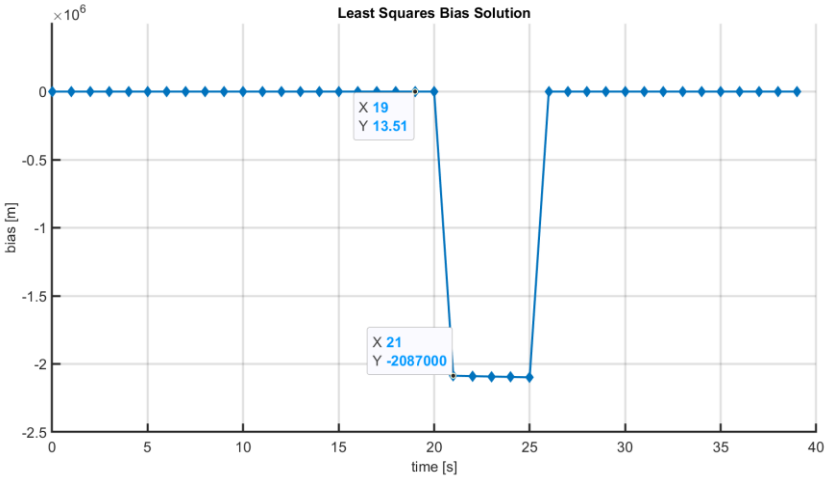

Figure 4-12 Least Squares Bias Solution

Similar to the position case, the least squares algorithm fails to provide an appropriate velocity and drift solution, which are obtained in Figure 4-13 and Figure 4-14.

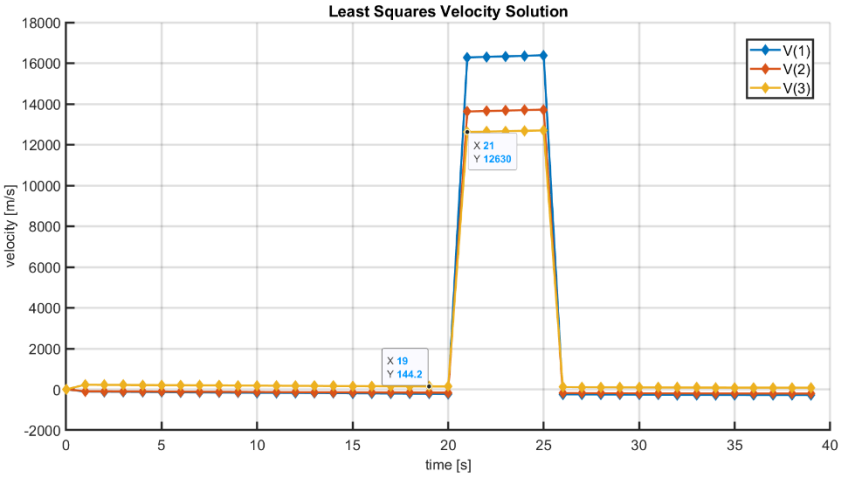

Figure 4-13 Least Squares Velocity Solution

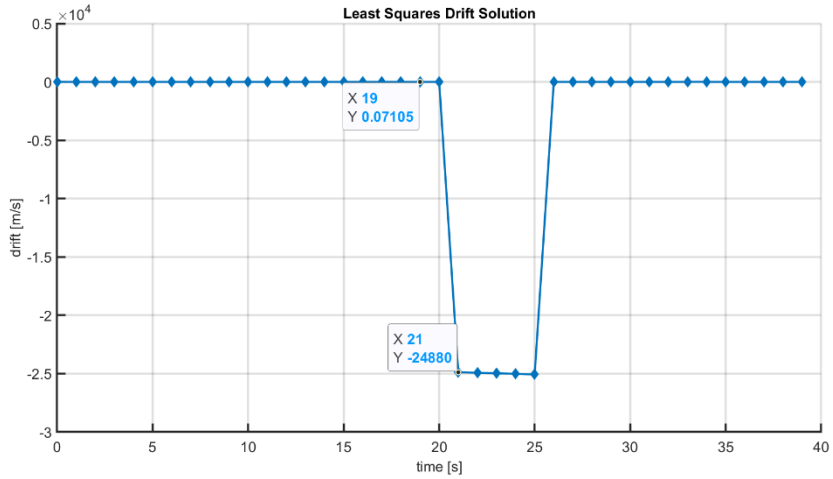

Figure 4-14 Least Squares Drift Solution

The investigation under faulty GPS measurements is done separately for loosely coupled and tightly coupled integration methods because the least squares algorithm cannot provide a proper navigation solution to use in loosely coupled integration. Solution errors are imposed directly in position and velocity for loosely coupled integration, as in Eq. (4.1).

$$[\varphi \quad \lambda \quad h] = [\varphi \quad \lambda \quad h] + [b_\varphi \quad b_\lambda \quad b_h] \tag{4.1}$$

$$[v_N \quad v_E \quad v_D] = [v_N \quad v_E \quad v_D] + [b_{v_N} \quad b_{v_E} \quad b_{v_D}] \tag{4.2}$$

For a tightly coupled integration method, the spoofing error is created by adding bias to the pseudo-range and pseudo-range rate measurements, as stated before.

$$\rho^m = \rho^m + b_\rho \tag{4.3}$$

$$\dot{\rho}^m = \dot{\rho}^m + b_{\dot{\rho}} \tag{4.4}$$

4.4.1 AKF with Loosely Coupled Integration

In case of faulty measurements from GPS, a statistical function to determine whether adaptive KF should be used or not is calculated and illustrated in Figure 4-15 for both SSF and MSF. As can be observed from the figure, β_k value is much higher for SSF than the MSF. In Figure 4-16 and Figure 4-17, SSF and MSF for position values are illustrated. The scale factor for the altitude is higher than the latitude and longitude.

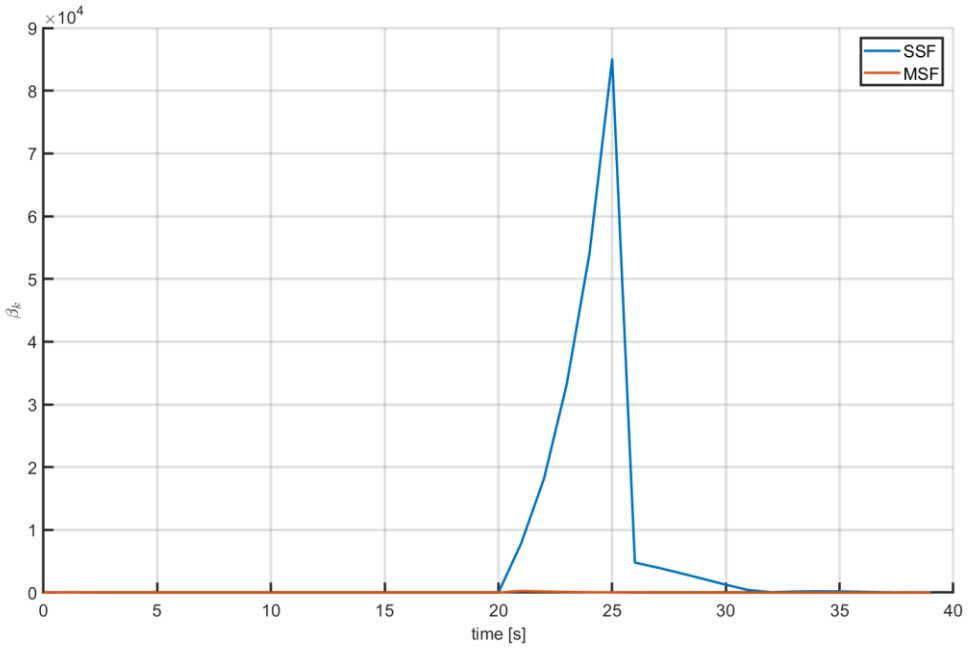

Figure 4-15 Statistical Function Value For Loosely Coupled Integration

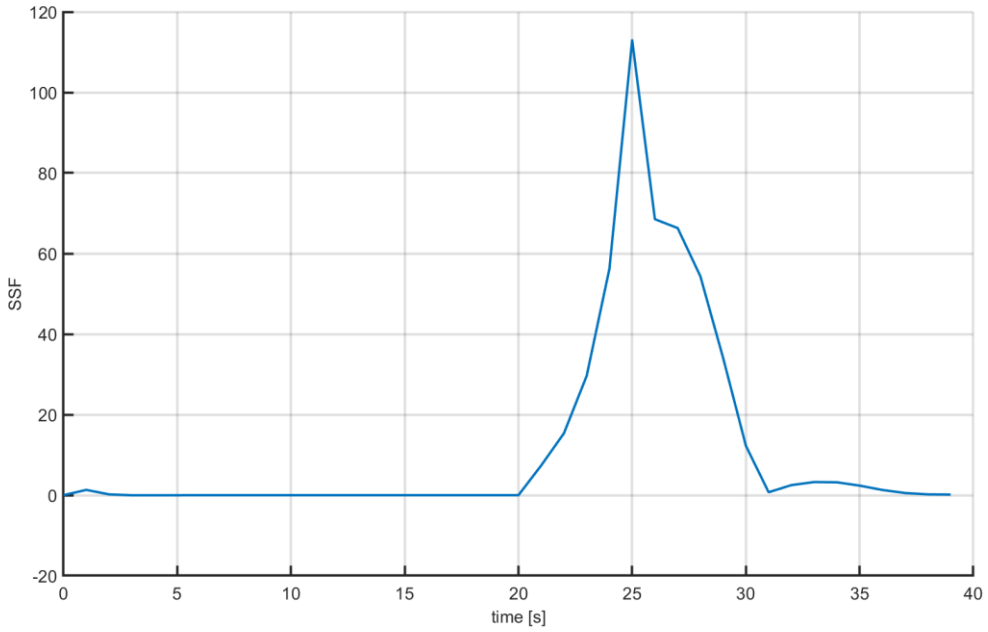

Figure 4-16 Single Scale Factor for Loosely Coupled Integration

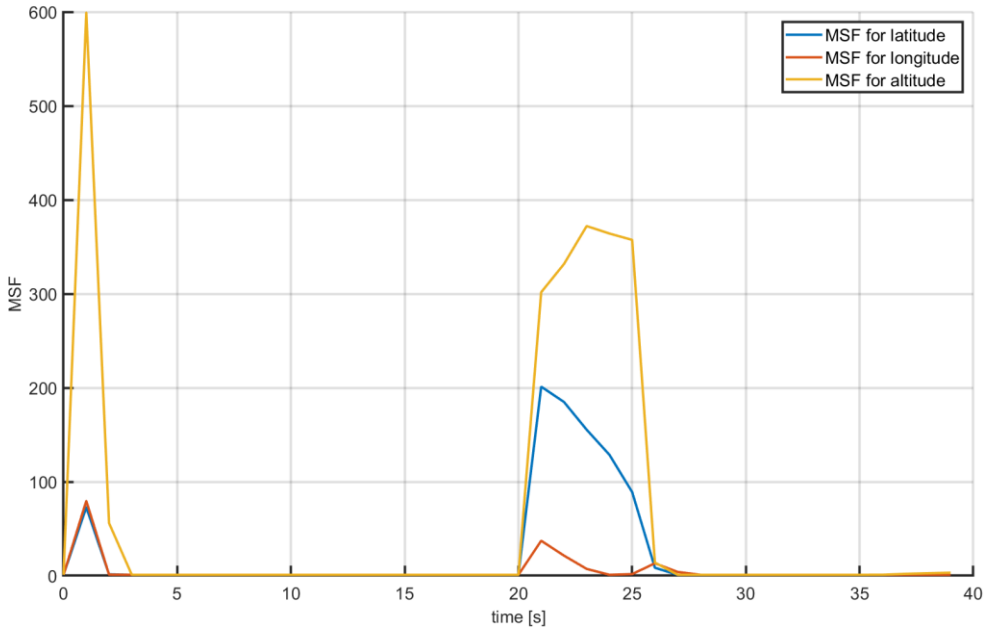

Figure 4-17 Multiple Scale Factors for Position

Figure 4-18, Figure 4-20, and Figure 4-21 show the navigation errors without adaptive filter and SSF and MSF. As can be observed from these figures, MSF gives the best results. MSF changes the measurement noise covariance matrix elements proportional to the error existing in that state. On the other hand, SSF multiplies the whole measurement noise covariance matrix with a scalar. In Figure 4-18, it is observed that when the GPS measurement error exists (between 20th and 25th seconds) and after the GPS error, MSF has the best position solutions. Even though SSF provides better position solutions compared to the case where AKF is not used during GPS error, after 25 seconds of the flight, their error magnitudes become almost the same.

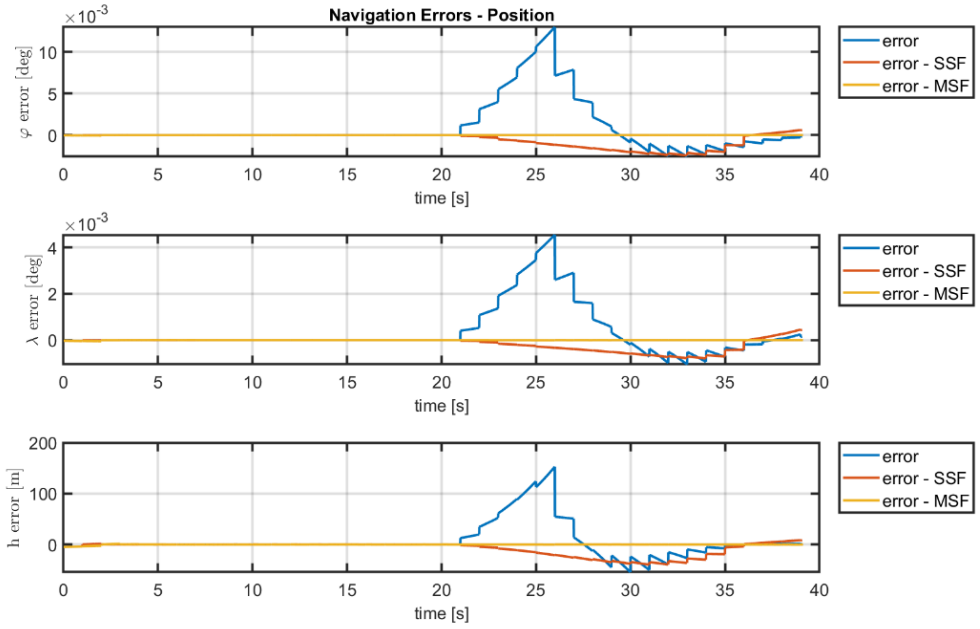

Figure 4-18 Loosely Coupled Integration Position Errors with AKF

Figure 4-19 shows the MSF values for velocity in loosely coupled integration for the guided munition. Since there exists a protection for the MSF values lower than 1. Even though the algorithm calculates the values lower than 1, the protection prevents them from having those values. Note that, in the case of GPS error for a loosely

coupled system, MSF for the velocities does not affect the elements related to the velocity in the measurement noise covariance matrix.

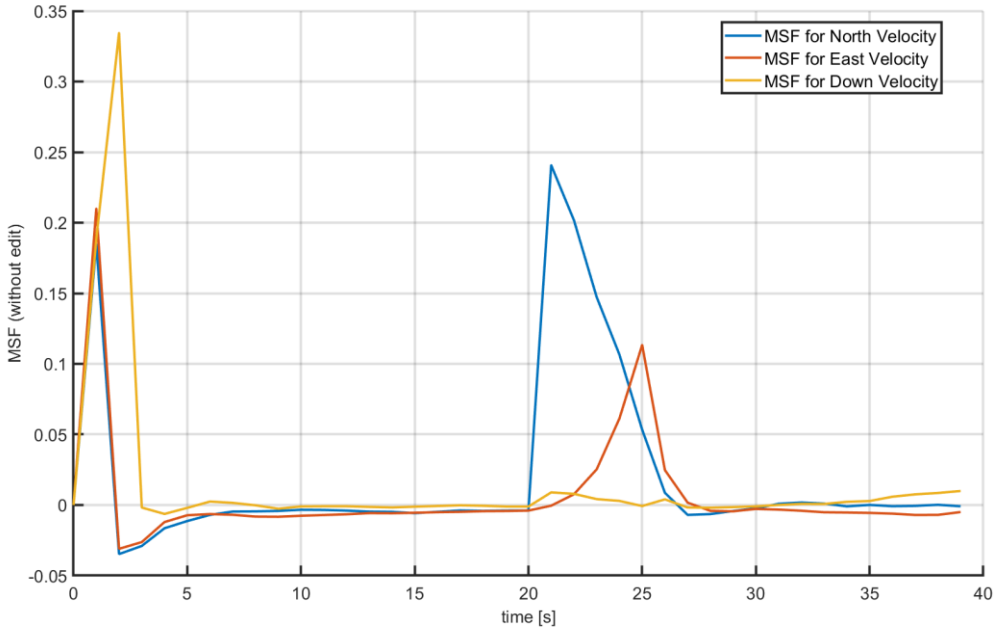

Figure 4-19 Multiple Scale Factors for Velocity

In Figure 4-20, it is observed during the whole flight, MSF has the best velocity solutions. SSF provides a better velocity solution compared to the GPS error case during flight. At the end of the flight, their errors become closer. It is concluded that their velocity errors converge to the same point if the flight time was longer.

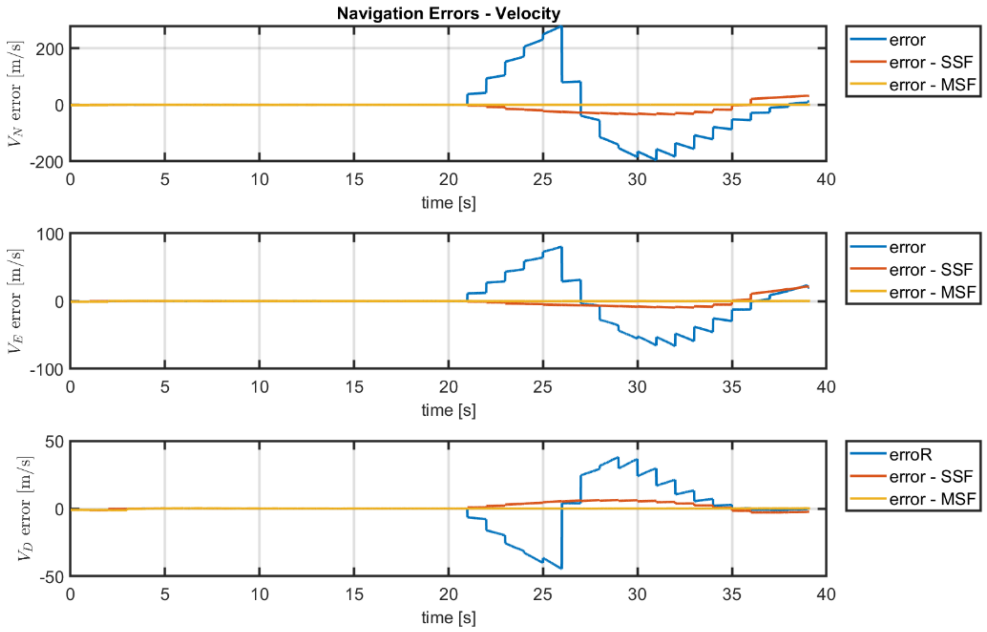

Figure 4-20 Loosely Coupled Integration Velocity Errors with AKF

In Figure 4-21, it is illustrated that MSF provides the best attitude solutions during the whole flight. SSF provides a better attitude solution compared to the GPS error case during flight. At the end of the flight, their errors become closer. It is concluded that if the flight time was longer, their attitude errors could converge to the same point.

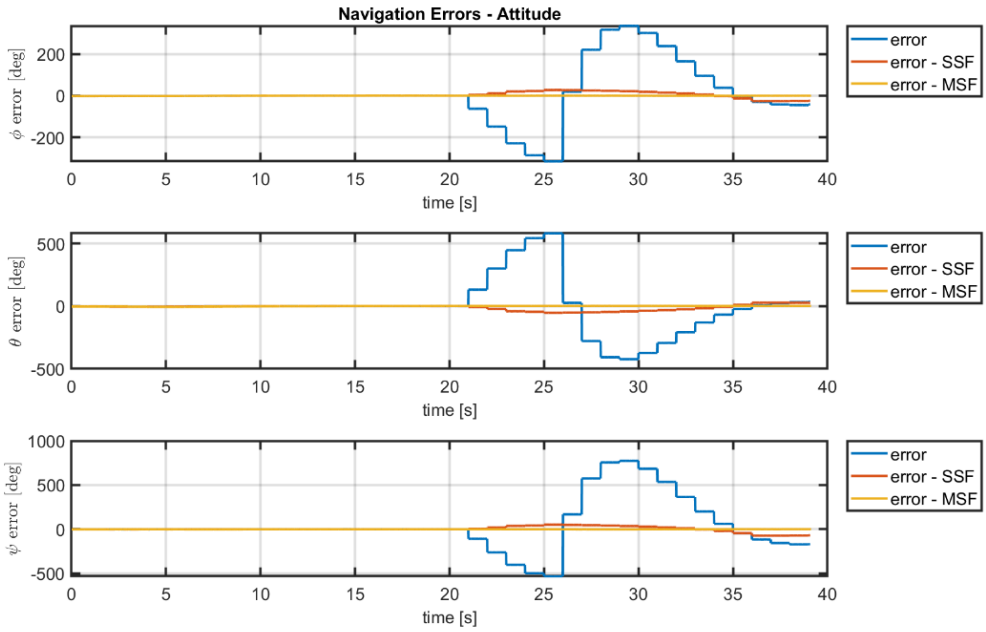

Figure 4-21 Loosely Coupled Integration Attitude Errors with AKF

Since the results of MSF cannot be observed from the above figures, separate figures are created to state how MSF produces the best navigation solutions in Figure 4-22, Figure 4-23, and Figure 4-24.

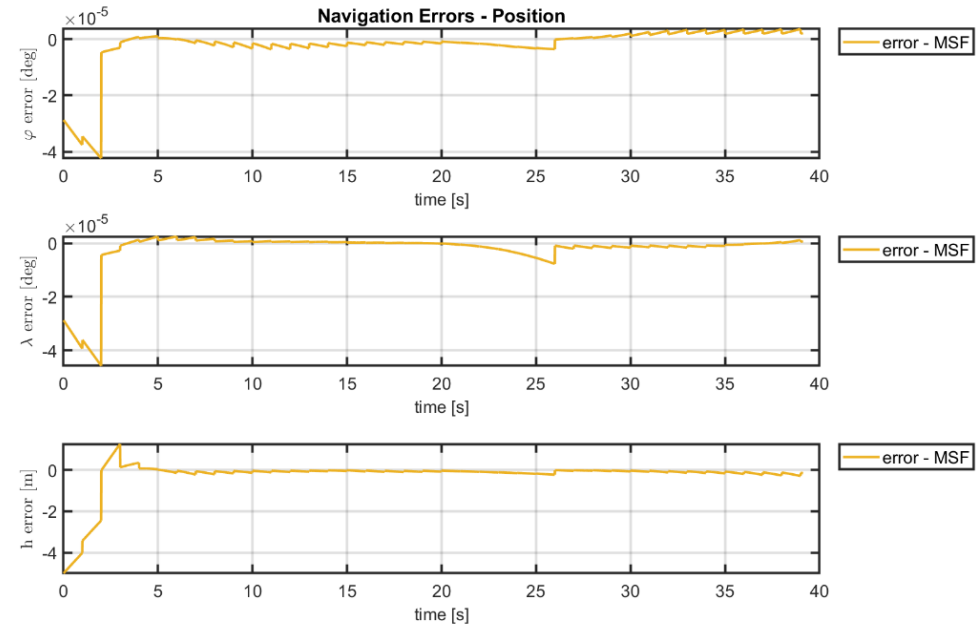

Figure 4-22 Loosely Coupled Integration Position Errors with MSF

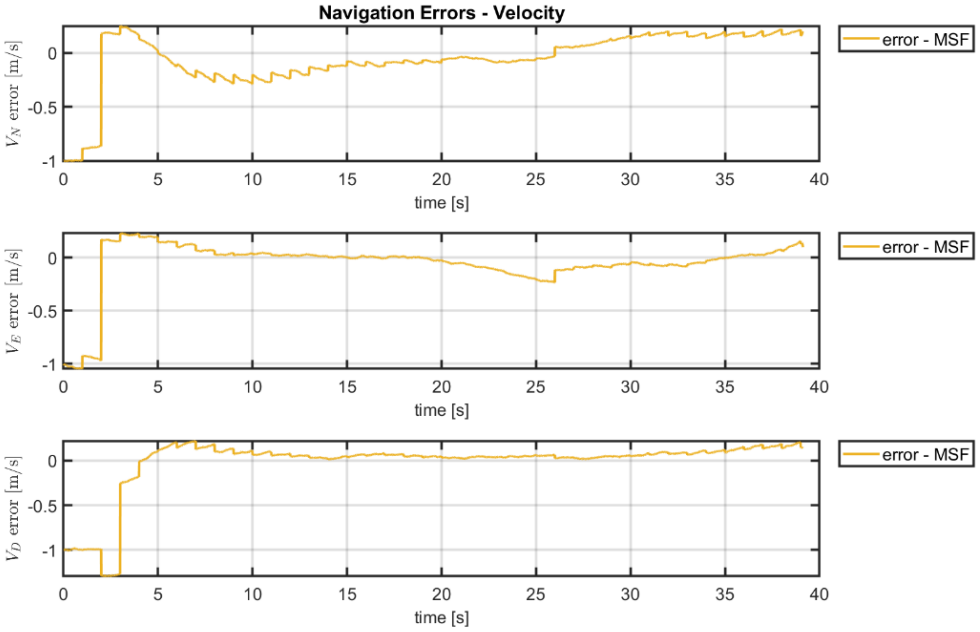

Figure 4-23 Loosely Coupled Integration Velocity Errors with MSF

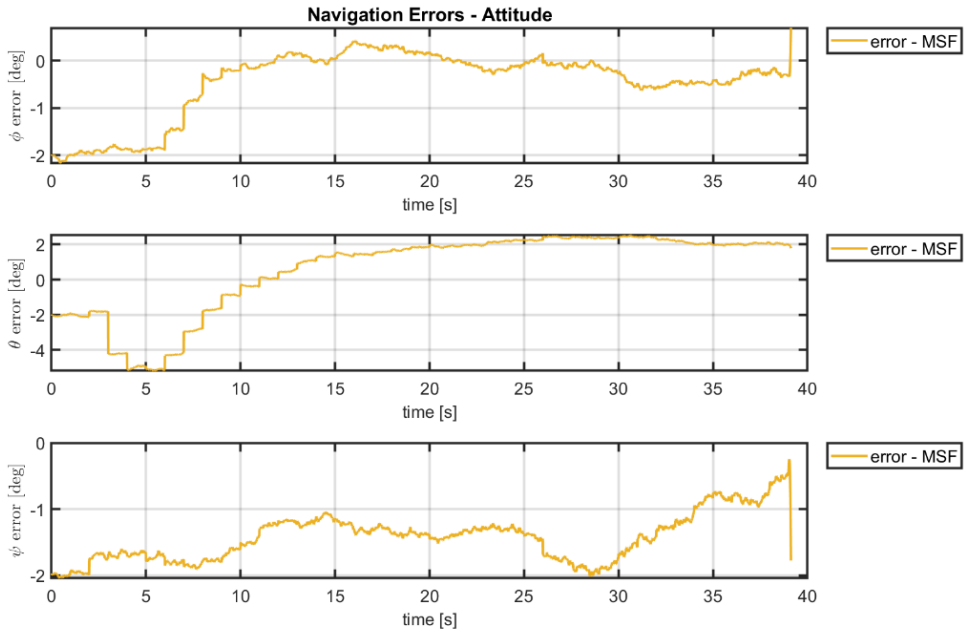

Figure 4-24 Loosely Coupled Integration Attitude Errors with MSF

4.4.2 AKF with Tightly Coupled Integration

In case of faulty measurements from GPS, a statistical function to determine whether adaptive KF should be used or not is calculated and illustrated in Figure 4-25 for both SSF and MSF. As can be observed from the figure, β_k value is similar for SSF and MSF in tightly coupled integration.

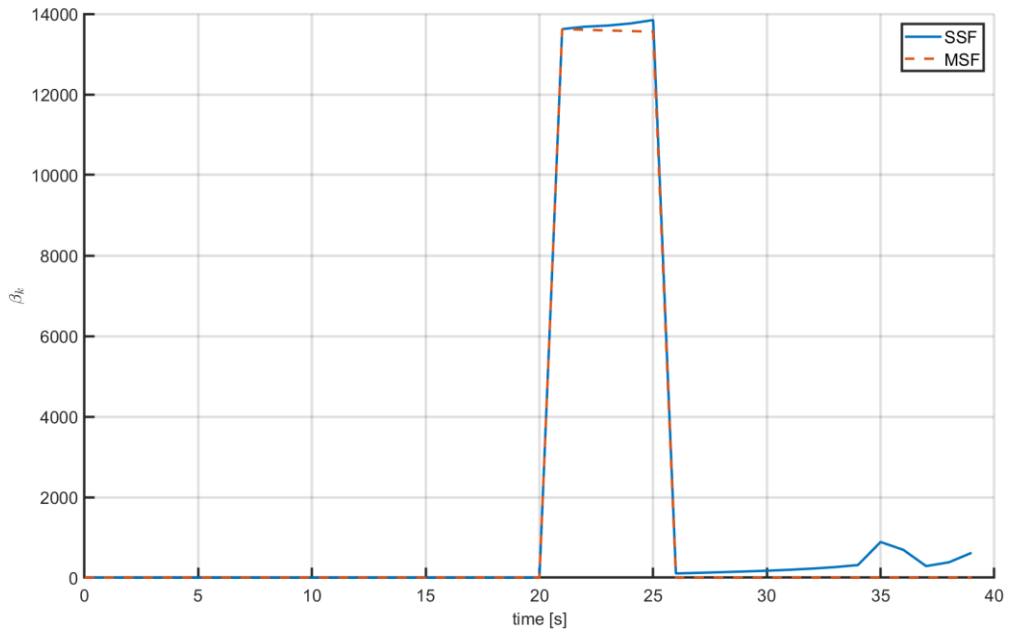

Figure 4-25 Statistical Function Value For Tightly Coupled Integration

In Figure 4-26 and Figure 4-27, SSF and MSF for pseudo-range values are illustrated. As can be observed from MSF values, the scale factor for the GPS number 5, which has the measurement error, is much higher than other satellites, as expected.

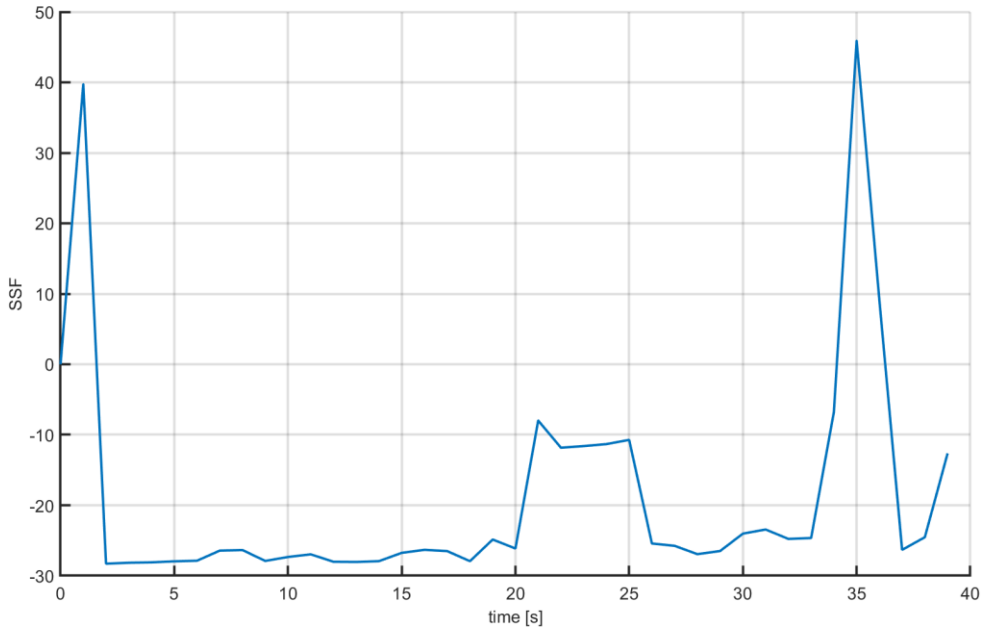

Figure 4-26 Single Scale Factor For Tightly Coupled Integration

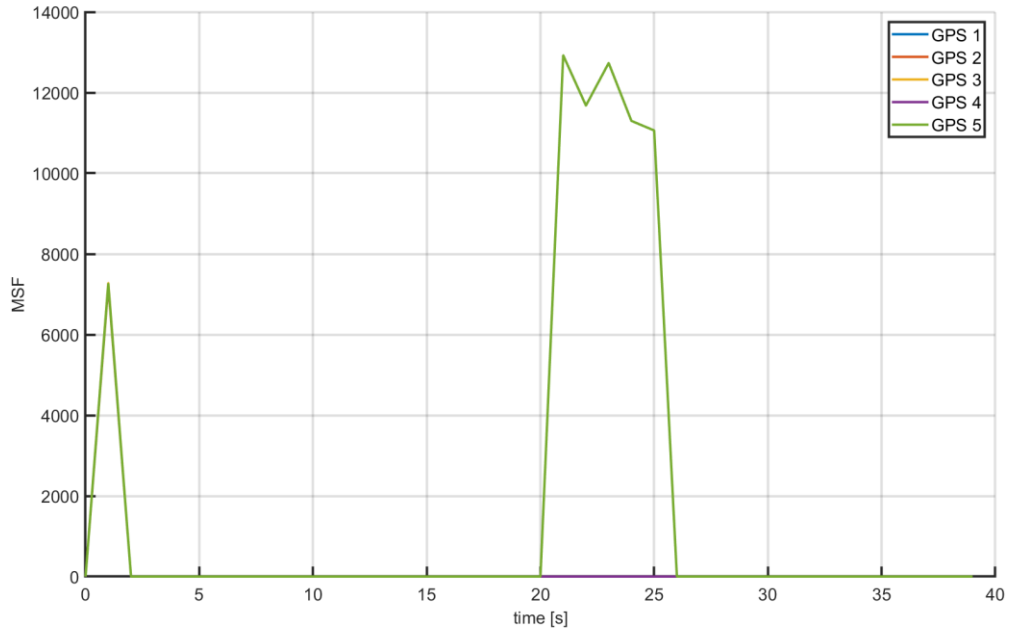

Figure 4-27 Multiple Scale Factors for Pseudo-Range Measurements

In case of faulty pseudo-range and pseudo-range rate measurements from GPS, Figure 4-28, Figure 4-30, and Figure 4-31 show the navigation errors without adaptive filter and SSF and MSF. As can be observed from these figures, MSF gives the best results. MSF changes the measurement noise covariance matrix elements proportional to the error existing in that state. On the other hand, SSF multiplies the whole measurement noise covariance matrix with a scalar. Figure 4-28 shows that SSF provides a better position solution during GPS error (between the 20th and 25th seconds of the flight) compared to the no AKF case; after a certain point, SSF position errors become larger than no AKF case.

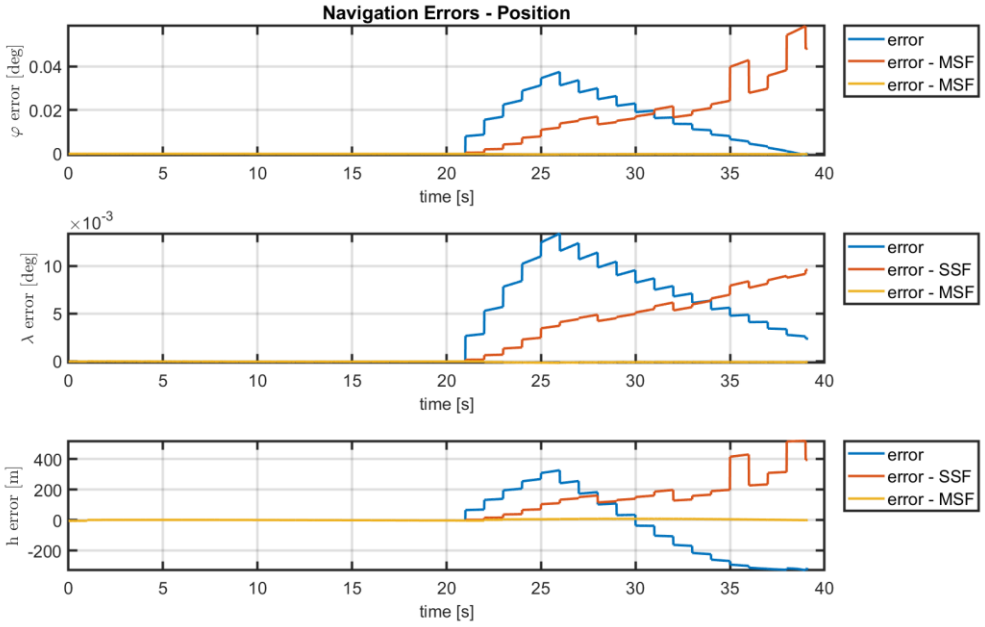

Figure 4-28 Tightly Coupled Integration Position Errors with AKF

Figure 4-29 shows the MSF values for pseudo-range rate measurements in tightly coupled integration for the guided munition. Since there exists a protection for the MSF values lower than 1. Even though the algorithm calculates the values lower than 1, the protection prevents them from having those values.

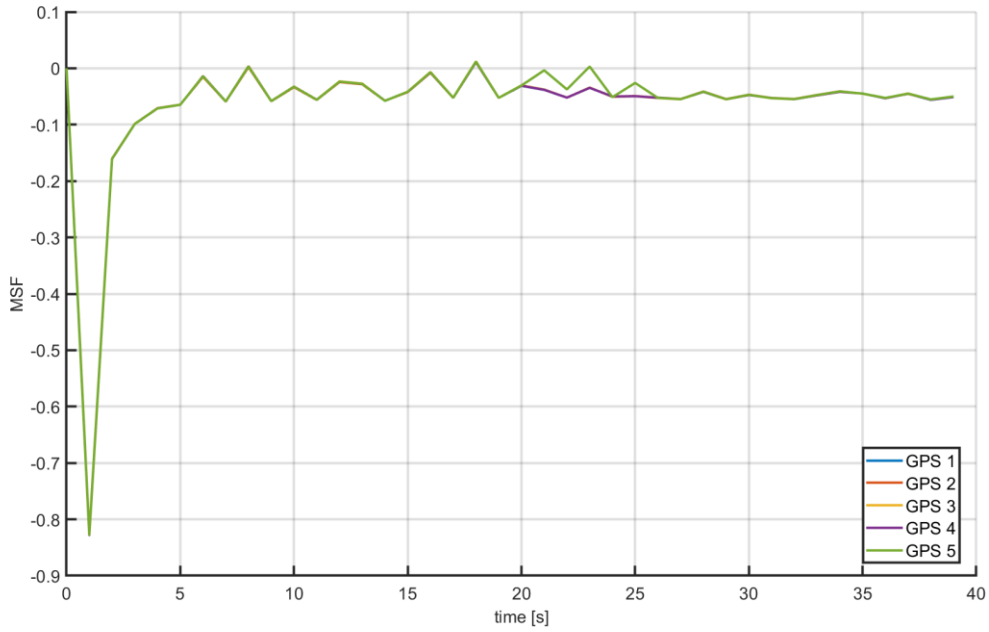

Figure 4-29 Multiple Scale Factors for Pseudo-Range Rate Measurements

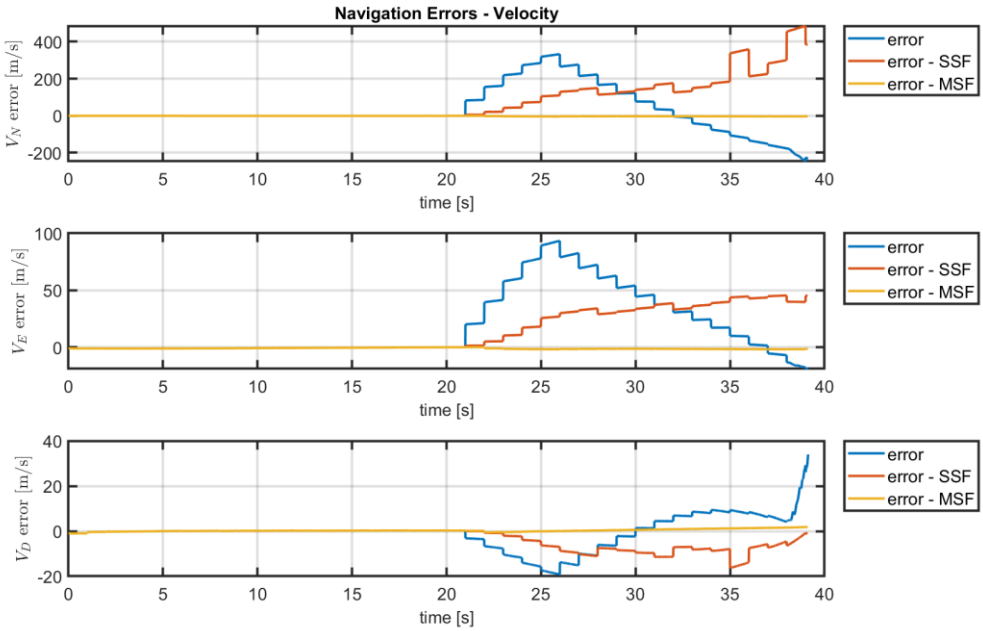

Figure 4-30 Tightly Coupled Integration Velocity Errors with AKF

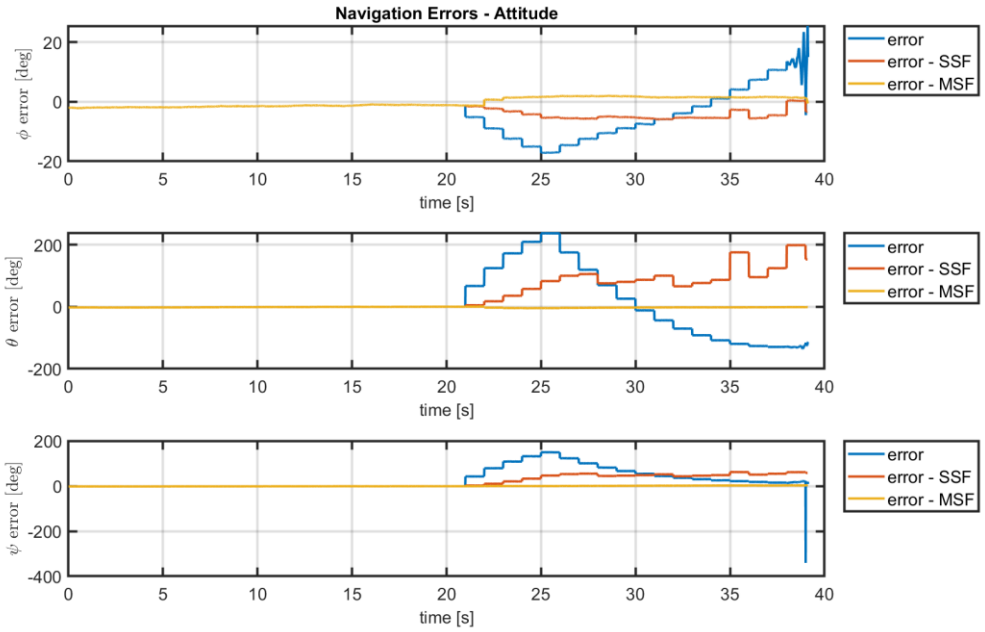

Figure 4-31 Tightly Coupled Integration Attitude Errors with AKF

Since the results of MSF cannot be observed from the above figures, separate figures are created to state how MSF produces the best navigation solutions in Figure 4-32, Figure 4-33, and Figure 4-34.

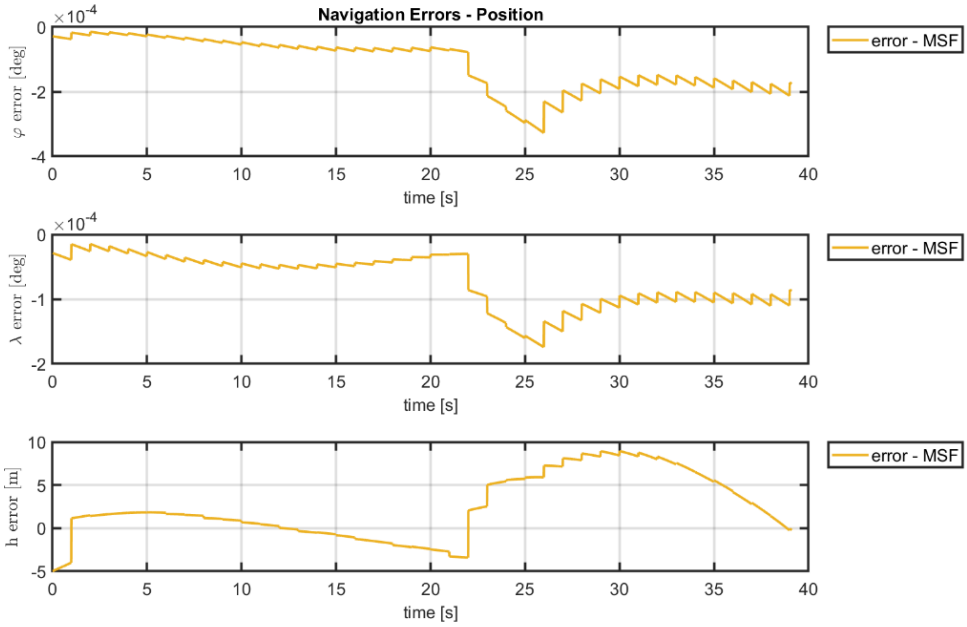

Figure 4-32 Tightly Coupled Integration Position Errors with MSF

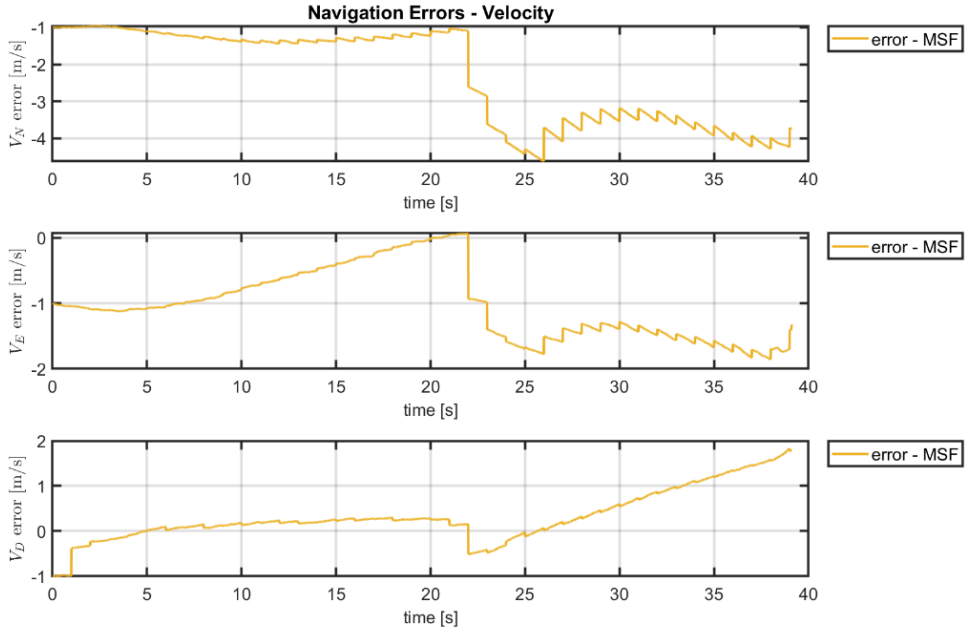

Figure 4-33 Tightly Coupled Integration Velocity Errors with MSF

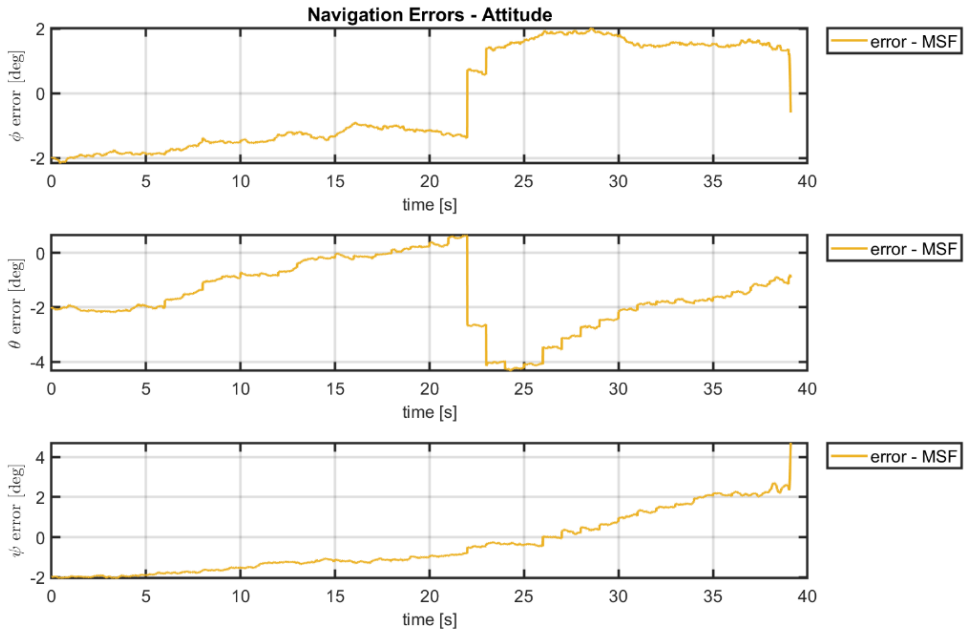

Figure 4-34 Tightly Coupled Integration Attitude Errors with MSF

CHAPTER 5

CONCLUSIONS

In this study, a simulation model for the guided munition is created to examine INS/GPS integration with different integration architectures, and adaptive KF is utilized to overcome GPS spoofing. Both loosely coupled and tightly coupled integration methods are applied, GPS spoofing is modeled, and navigation errors are illustrated for all cases. In the case of GPS spoofing, AKF is achieved with both SSF and MSF. Since MSF adapts the diagonal elements of the measurement noise covariance matrices, it has some advantages over SSF. Loosely coupled and tightly coupled integration methods differ in measurment models and this results in calculated MSF affect different types of measurements. In loosely coupled integration, MSF adapts the position and velocity elements of the measurement noise covariance matrix. In tightly coupled integration, pseudo-range and pseudo range rate measurements are affected by MSF. This study shows that, while single scale factor could be used for loosely coupled integration, it şs not suggested for the tightly coupled integartion method. Because when a measurement is faulty in loosely coupled system it affects all position and velocity information and multiplying a SSF with measurement noise covariance matrix is acceptable. On the other hand, if only one of the GPS measurements are faulty in tightly coupled integration, it does not affect all measurements. In that case, if SSF is multiplied with measurement noise covariance matrix, the result is losing the valuable information from other satelleties. When GPS spoofing results in malfunction only position or only velocity, adapting the related element preserves the important information to be lost completely.

REFERENCES

[1] “precision-guided munition,” *Dod Dictionary of Military and Associated Terms*. Joint Chiefs of Staff, Washington, D.C., pp. 170–170, 2020

[2] J. R. Hoehn, “Precision-guided munitions: Background and issues for Congress,” Defence Technical Information Center, https://crsreports.congress.gov/product/pdf/r/r45996 (accessed Aug. 17, 2023).

[3] A. Noureldin, T. B. Karamat, and J. Georgy, *Fundamentals of Inertial Navigation, Satellite-Based Positioning and Their Integration*. Berlin, Heidelberg: Springer, 2013.

[4] D. H. Titterton and J. L. Weston, *Strapdown Inertial Navigation Technology*. Reston: American Institute of Aeronautics and Astronautics, 2004.

[5] P. Groves, *Principles of GNSS, Inertial, and Multi-Sensor Integrated Navigation Systems*. Boston, Massachusetts: Artech House, 2008.

[6] M. S. Grewal, A. P. Andrews, and C. Bartone, *Global Positioning Satellite Systems, Inertial Navigation, and Integration*. Hoboken, NJ: Wiley-Blackwell, 2013.

[7] N. Y. Ko and T. G. Kim, “Comparison of kalman filter and particle filter used for localization of an underwater vehicle,” *2012 9th International Conference on Ubiquitous Robots and Ambient Intelligence (URAI)*, 2012. doi:10.1109/urai.2012.6463013

[8] M. St-Pierre and D. Gingras, “Comparison between the unscented Kalman filter and the extended Kalman filter for the position estimation module of an Integrated Navigation Information System,” *IEEE Intelligent Vehicles Symposium, 2004*, 2004. doi:10.1109/ivs.2004.1336492

[9] Tang. P. Van, Thang. N. Van, D. Anh. Nguyen, Trinh. C. Duc, and Tan. T. Duc, “15-state extended Kalman filter design for INS/GPS Navigation System,” *Journal*

of Automation and Control Engineering, vol. 3, no. 2, pp. 109–114, 2015. doi:10.12720/joace.3.2.109-114

[10] V. Madyastha, V. Ravindra, S. Mallikarjunan, and A. Goyal, "Extended Kalman filter vs. error state kalman filter for aircraft attitude estimation," *AIAA Guidance, Navigation, and Control Conference*, 2011. doi:10.2514/6.2011-6615

[11] E. Ohlmeyer, T. Pepitone, and B. Miller, "Assesment of integrated GPS/INS for the EX-171 extended range guided munition," *Guidance, Navigation, and Control Conference and Exhibit*, 1998. doi:10.2514/6.1998-4416

[12] G. T. Schmidt, *INS/GPS Integration Architecture Performance Comparisons*, 2010.

[13] A. H. Mohamed and K. P. Schwarz, "Adaptive Kalman filtering for INS/GPS," *Journal of Geodesy*, vol. 73, no. 4, pp. 193–203, 1999. doi:10.1007/s001900050236

[14] Hajiyev, C., Soken, H.E. (2016). Fault Tolerant Estimation of UAV Dynamics via Robust Adaptive Kalman Filter. In: Dimirovski, G. (eds) Complex Systems. Studies in Systems, Decision and Control, vol 55. Springer, Cham. https://doi.org/10.1007/978-3-319-28860-4_17

[15] B. Etkin, *Dynamics of Atmospheric Flight*. Mineola, NY: Dover Publications, Inc., 2019.

[16] B. L. Stevens, F. L. Lewis, and E. N. Johnson, *Aircraft Control and Simulation: Dynamics, Controls Design, and Autonomous Systems*. Hoboken, NJ: Wiley, 2016.

[17] G. M. Siouris, *Missile Guidance and Control Systems*. New York, NY: Springer, 2011.

[18] "ECEF Position to LLA," Calculate geodetic latitude, longitude, and altitude above planetary ellipsoid from Earth-centered Earth-fixed (ECEF) position - Simulink, https://www.mathworks.com/help/aeroblks/ecefpositiontolla.html.

[19] H. D. Curtis, *Orbital Mechanics for Engineering Students: Revised Fourth Edition*. Amsterdam: Elsevier, 2021.

[20] K. Ogata, *Modern Control Engineering*. Delhi: Pearson, 2016.

[21] N. F. Palumbo, "Basic Principles of Homing Guidance," *Johns Hopkins Apl Technical Digest* , vol. 10, no. 1, 2010.

[22] E.-H. Shin, "Accuracy improvement of low cost INS/GPS for Land Applications," thesis, National Library of Canada = Bibliothèque nationale du Canada, Ottawa, 2003

APPENDICES

A. Least Squares Method

The least squares algorithm is applied to obtain the position and velocity measurements of the GPS by using pseudo-range and pseudo-range rate measurements. These position and velocity solutions are necessary in the loosely coupled integration method. The algorithm is based on using minimum of four satellites' measurements and estimating GPS position, bias, velocity, and drift as follows [3]:

$$\begin{bmatrix} \delta\rho^1 \\ \vdots \\ \delta\dot{\rho}^M \\ \delta\dot{\rho}^1 \\ \vdots \\ \delta\dot{\rho}^M \end{bmatrix} = \begin{bmatrix} (1_{est}^1)^T & 1 & 0_{3x1} & 0 \\ \vdots & \vdots & \vdots & \vdots \\ (1_{est}^1)^T & 1 & 0_{3x1} & 0 \\ 0_{3x1} & 0 & (1_{est}^1)^T & 1 \\ \vdots & \vdots & \vdots & \vdots \\ 0_{3x1} & 0 & (1_{est}^M)^T & 1 \end{bmatrix} \begin{bmatrix} \delta r \\ \delta b \\ \delta v \\ \delta d \end{bmatrix} + \begin{bmatrix} \varepsilon_\rho^1 \\ \vdots \\ \varepsilon_\rho^M \\ \varepsilon_{\dot{\rho}}^1 \\ \vdots \\ \varepsilon_{\dot{\rho}}^M \end{bmatrix} \quad (A.1)$$

$$\delta z_{2Mx1} = G_{2Mx8}\delta S_{8x1} + \varepsilon_{2Mx1} \quad (A.2)$$

If there are four or more satellites, the least squares solution as in Eq. (A.3):

$$\delta S = (G^T G)^{-1} G^T \delta z \quad (A.3)$$

$$r_{est,k} = r_{est,k-1} + \delta r \quad (A.4)$$

$$b_{est,k} = b_{est,k-1} + \delta b \quad (A.5)$$

$$\delta v_{est,k} = \delta v_{est,k} + \delta v \quad (A.6)$$

$$d_{est,k} = \delta d_{est,k-1} + \delta d \quad (A.7)$$

This algorithm is repeated, until δS is in the given tolerances [3]. Then, the GPS position and velocity solutions are obtained to be used in loosely coupled INS/GPS integration.

B. Derivation of Linear Autopilot Matrices

The linear autopilot matrices are created by using force and moment equations acting on a flying vehicle. The forces acting on a body include aerodynamical and gravitational forces as stated in Eq. (B.1) [16]:

$$F_{aero} + F_{grav} = m\left(\dot{v}_{eb}^{b} + \omega_{ib}^{b} \times v_{eb}^{b}\right) \tag{B.1}$$

$$\begin{bmatrix} X \\ Y \\ Z \end{bmatrix} + C_n^b \, m \begin{bmatrix} 0 \\ 0 \\ g \end{bmatrix} = m\left(\begin{bmatrix} \dot{u} \\ \dot{v} \\ \dot{w} \end{bmatrix} + \begin{bmatrix} 0 & -r & q \\ r & 0 & -p \\ -q & p & 0 \end{bmatrix} \begin{bmatrix} u \\ v \\ w \end{bmatrix}\right) \tag{B.2}$$

$$X - mg\sin\theta = m(\dot{u} + qw - rv) \tag{B.3}$$

$$Y + mg\cos\theta\sin\phi = m(\dot{v} + ru - pw) \tag{B.4}$$

$$Z + mg\cos\theta\cos\phi = m(\dot{w} + pv - qu) \tag{B.5}$$

The moments acting on a flying vehicle are stated in Eq. (B.6) [16]:

$$M^b = \dot{I}^b \omega_{ib}^b + I^b \dot{\omega}_{ib}^b + \omega_{ib}^b \times I^b \omega_{ib}^b \tag{B.6}$$

$$\begin{aligned} \begin{bmatrix} L \\ M \\ N \end{bmatrix} = &\begin{bmatrix} \dot{I}_{xx} & -\dot{I}_{xy} & -\dot{I}_{zx} \\ -\dot{I}_{xy} & \dot{I}_{yy} & -\dot{I}_{yz} \\ -\dot{I}_{zx} & -\dot{I}_{yz} & \dot{I}_{zz} \end{bmatrix} \begin{bmatrix} p \\ q \\ r \end{bmatrix} + \begin{bmatrix} I_{xx} & -I_{xy} & -I_{zx} \\ -I_{xy} & I_{yy} & -I_{yz} \\ -I_{zx} & -I_{yz} & I_{zz} \end{bmatrix} \begin{bmatrix} p \\ q \\ r \end{bmatrix} \\ &+ \begin{bmatrix} 0 & -r & q \\ r & 0 & -p \\ -q & p & 0 \end{bmatrix} \begin{bmatrix} I_{xx} & -I_{xy} & -I_{zx} \\ -I_{xy} & I_{yy} & -I_{yz} \\ -I_{zx} & -I_{yz} & I_{zz} \end{bmatrix} \begin{bmatrix} p \\ q \\ r \end{bmatrix} \end{aligned} \tag{B.7}$$

Note that, for a guided munition $I_{xz} \approx I_{yz} \approx I_{xy} \approx 0$ since it is symmetric wrt two axes and also by taking small inertia change, $\dot{\vec{I}}^{(b)} \approx 0$, equations become:

$$L = I_x \dot{p} - \left(I_{yy} - I_{zz}\right) qr \tag{B.8}$$

$$M = I_y \dot{q} - (I_{zz} - I_{xx}) rp \tag{B.9}$$

$$N = I_z \dot{r} - \left(I_{xx} - I_{yy}\right) pq \tag{B.10}$$

For the pitch dynamics, the definition of angle of attack is the starting point of creating the linear matrices.

$$\alpha = \arctan\left(\frac{w}{u}\right) \tag{B.11}$$

For small angle of attack assumption:

$$\alpha \approx \frac{w}{u} \tag{B.12}$$

$$\dot{\alpha} = \frac{\dot{w}u - w\dot{u}}{u^2} \tag{B.13}$$

Instead of $\dot{w}$ expression from Eq. (B.5) is used:

$$\dot{\alpha} = \frac{\left(\frac{Z}{m} + qu\right)u - w\dot{u}}{u^2} \tag{B.14}$$

Note that Z-force can be expressed in terms of aerodynamic derivatives and some parameteres as in Eq. (B.15):

$$Z = Z_\alpha \alpha + Z_q q + Z_\delta \delta \tag{B.15}$$

$$\dot{\alpha} = \left(\frac{Z_\alpha}{mu} - \frac{\dot{u}}{u}\right)\alpha + \left(\frac{Z_q}{mu} + 1\right)q + \frac{Z_\delta}{mu}\delta \tag{B.16}$$

For $r = p = 0$, from Eq. (B.9):

$$\dot{q} = \frac{M}{I_y} \tag{B.17}$$

Note that M-moment can be expressed in terms of aerodynamic derivatives and some parameteres as in Eq. (B.18):

$$M = M_\alpha \alpha + M_q q + M_\delta \delta \tag{B.18}$$

Putting Eq. (B.18) into the Eq. (B.17):

$$\dot{q} = \frac{M_\alpha}{I_y}\alpha + \frac{M_q}{I_y}q + \frac{M_\delta}{I_y}\delta \tag{B.19}$$

Finally acceleration in z direction is found by dividing the Z-force to the guided munition's mass:

$$a_Z = \frac{Z_\alpha}{m}\alpha + \frac{Z_q}{m}q + \frac{Z_\delta}{m}\delta \qquad (B.20)$$

$$\dot{a}_Z = \frac{Z_\alpha}{m}\dot{\alpha} + \frac{Z_q}{m}\dot{q} + \frac{Z_\delta}{m}\dot{\delta} \qquad (B.21)$$

$$\begin{aligned}\dot{a}_Z = \frac{Z_\alpha}{m}\left(\left(\frac{Z_\alpha}{mu} - \frac{\dot{u}}{u}\right)\alpha + \left(\frac{Z_q}{mu} + 1\right)q + \frac{Z_\delta}{mu}\delta\right) \\ + \frac{Z_q}{m}\left(\frac{M_\alpha}{I_y}\alpha + \frac{M_q}{I_y}q + \frac{M_\delta}{I_y}\delta\right) + \frac{Z_\delta}{m}\dot{\delta}\end{aligned} \qquad (B.22)$$

With the manipulation of Eq. (B.20) angle of attack becomes:

$$\alpha = \frac{m}{Z_\alpha}a_z - \frac{Z_q}{Z_\alpha}q - \frac{Z_\delta}{Z_\alpha}\delta \qquad (B.23)$$

Putting Eq. (B.23) into the Eq. (B.22):

$$\begin{aligned}\dot{a}_Z = \left(\frac{Z_\alpha}{mu} + \frac{Z_q M_\alpha}{Z_\alpha I_y} - \frac{\dot{u}}{u}\right)a_Z + \left(\frac{Z_\alpha}{m} + \frac{Z_q\dot{u}}{mu} + \frac{Z_q M_q}{mI_y} - \frac{Z_q^2 M_\alpha}{Z_\alpha m I_y}\right)q \\ + \left(\frac{Z_\delta\dot{u}}{mu} - \frac{Z_q M_\alpha Z_\delta}{Z_\alpha m I_y} + \frac{Z_q M_\delta}{mI_y}\right)\delta + \frac{Z_\delta}{m}\dot{\delta}\end{aligned} \qquad (B.24)$$

Putting Eq. (B.23) into the Eq. (B.19):

$$\dot{q} = \left(\frac{M_\alpha m}{I_y Z_\alpha}\right)a_Z + \left(\frac{M_q}{I_y} - \frac{M_\alpha Z_q}{Z_\alpha I_y}\right)q + \left(\frac{M_\delta}{I_y} - \frac{M_\alpha Z_\delta}{Z_\alpha I_y}\right)\delta \qquad (B.25)$$

By adding the CAS dynamics into the system linear matrices for the pitch dynamics can be written as in Eq (B.26):

$$\begin{bmatrix} \dot{a}_Z \\ \dot{q} \\ \dot{\delta} \\ \ddot{\delta} \end{bmatrix} = \begin{bmatrix} \frac{Z_\alpha}{mu} + \frac{Z_q M_\alpha}{Z_\alpha I_y} - \frac{\dot{u}}{u} & \frac{Z_\alpha}{m} + \frac{Z_q \dot{u}}{mu} + \frac{Z_q M_q}{m I_y} - \frac{Z_q^2 M_\alpha}{Z_\alpha m I_y} & \frac{Z_\delta \dot{u}}{mu} - \frac{Z_q M_\alpha Z_\delta}{Z_\alpha m I_y} + \frac{Z_q M_\delta}{m I_y} & \frac{Z_\delta}{m} \\ \frac{M_\alpha m}{I_y Z_\alpha} & \frac{M_q}{I_y} - \frac{M_\alpha Z_q}{Z_\alpha I_y} & \frac{M_\delta}{I_y} - \frac{M_\alpha Z_\delta}{Z_\alpha I_y} & 0 \\ 0 & 0 & 0 & 1 \\ 0 & 0 & -\omega_n^2 & -2\zeta\omega_n^2 \end{bmatrix} \begin{bmatrix} a_Z \\ q \\ \delta \\ \dot{\delta} \end{bmatrix} + \begin{bmatrix} 0 \\ 0 \\ 0 \\ \omega_n^2 \end{bmatrix} \delta_c \qquad (B.26)$$

For the yaw dynamics, the definition of sideslip angle is the starting point of creating the linear matrices.

$$\beta = \arcsin\left(\frac{v}{V}\right) \qquad (B.27)$$

For small sideslip angle assumption:

$$\beta \approx \frac{v}{V} \qquad (B.28)$$

Time derivative of the sideslip angle isgiven in Eq. (B.29):

$$\dot{\beta} = \frac{\dot{v}V - v\dot{V}}{V^2} \qquad (B.29)$$

Instead of $\dot{v}$ expression from Eq. (B.4) is used:

$$\dot{\beta} = \frac{\left(\frac{Y}{m} - ru\right)V - v\dot{V}}{V^2} \qquad (B.30)$$

Note that Y-force can be expressed in terms of aerodynamic derivatives and some parameteres as in Eq. (B.31):

$$Y = Y_\beta \beta + Y_r r + Y_\delta \delta \qquad (B.31)$$

Assuming that, munition has biggest velocity in the x direction. Hence $u \approx V$ Eq. (B.30) becomes:

$$\dot{\beta} = \left(\frac{Y_\beta}{mV} - \frac{\dot{V}}{V}\right)\beta + \left(\frac{Y_r}{mV} - 1\right)r + \frac{Y_\delta}{mV}\delta \qquad (B.32)$$

For $p = q = 0$, Eq. (B.10):

$$\dot{r} = \frac{N}{I_z} \tag{B.33}$$

Note that N-moment can be expressed in terms of aerodynamic derivatives and some parameteres as in Eq. (B.34):

$$N = N_\beta \beta + N_r r + N_\delta \delta \tag{B.34}$$

Putting Eq. (B.34) into the Eq. (B.33):

$$\dot{r} = \frac{N_\beta}{I_z}\beta + \frac{N_r}{I_z} r + \frac{N_\delta}{I_z}\delta \tag{B.35}$$

Finally acceleration in y direction is found by dividing the Y-force to the guided munition's mass:

$$a_Y = \frac{Y_\beta}{m}\beta + \frac{Y_r}{m} r + \frac{Y_\delta}{m}\delta \tag{B.36}$$

$$\dot{a}_Y = \frac{Y_\beta}{m}\dot{\beta} + \frac{Y_r}{m}\dot{r} + \frac{Y_\delta}{m}\dot{\delta} \tag{B.37}$$

$$\begin{aligned} \dot{a}_Y = \frac{Y_\beta}{m}\left(\left(\frac{Y_\beta}{mV} - \frac{\dot{V}}{V}\right)\beta + \left(\frac{Y_r}{mV} - 1\right) r + \frac{Y_\delta}{mV}\delta\right) \\ + \frac{Y_r}{m}\left(\frac{N_\beta}{I_z}\beta + \frac{N_r}{I_z} r + \frac{N_\delta}{I_z}\delta\right) + \frac{Y_\delta}{m}\dot{\delta} \end{aligned} \tag{B.38}$$

With the manipulation of $Eq.(C.36)$ sideslip angle becomes:

$$\beta = \frac{m}{Y_\beta} a_Y - \frac{Y_r}{Y_\beta} r - \frac{Y_\delta}{Y_\beta}\delta \tag{B.39}$$

Putting Eq. (B.39) into the Eq. (B.38):

$$\begin{aligned} \dot{a}_Y = \left(\frac{Y_\beta}{mV} + \frac{Y_r N_\beta}{Y_\beta I_z} - \frac{\dot{V}}{V}\right) a_Y + \left(-\frac{Y_\beta}{m} + \frac{Y_r \dot{V}}{mV} + \frac{Y_r N_r}{m I_z} - \frac{Y_r^2 N_\beta}{Y_\beta m I_z}\right) r \\ + \left(\frac{Y_\delta \dot{V}}{mV} - \frac{Y_r N_\beta Y_\delta}{Y_\beta m I_z} + \frac{Y_r N_\delta}{m I_z}\right)\delta + \frac{Y_\delta}{m}\dot{\delta} \end{aligned} \tag{B.40}$$

Putting Eq. (B.39) into the Eq. (B.35):

$$\dot{r} = \left(\frac{N_\beta m}{Y_\beta I_z}\right) a_Y + \left(\frac{N_r}{I_z} - \frac{N_\beta Y_r}{Y_\beta I_z}\right) r + \left(\frac{N_\delta}{I_z} - \frac{N_\beta Y_\delta}{Y_\beta I_z}\right) \delta \qquad (B.41)$$

By adding the CAS dynamics into the system linear matrices for the yaw dynamics can be written as in Eq (B.42):

$$\begin{bmatrix} \dot{a_Y} \\ \dot{r} \\ \dot{\delta} \\ \ddot{\delta} \end{bmatrix} = \begin{bmatrix} \frac{Y_\beta}{mV} + \frac{Y_r N_\beta}{Y_\beta I_z} - \frac{\dot{V}}{V} & -\frac{Y_\beta}{m} + \frac{Y_r \dot{V}}{mV} + \frac{Y_r N_r}{m I_z} - \frac{Y_r^2 N_\beta}{Y_\beta m I_z} & \frac{Y_\delta \dot{V}}{mV} - \frac{Y_r N_\beta Y_\delta}{Y_\beta m I_z} + \frac{Y_r N_\delta}{m I_z} & \frac{Y_\delta}{m} \\ \frac{N_\beta m}{Y_\beta I_z} & \frac{N_r}{I_z} - \frac{N_\beta Y_r}{Y_\beta I_z} & \frac{N_\delta}{I_z} - \frac{N_\beta Y_\delta}{Y_\beta I_z} & 0 \\ 0 & 0 & 0 & 1 \\ 0 & 0 & -\omega_n^2 & -2\zeta\omega_n^2 \end{bmatrix} \begin{bmatrix} a_Y \\ r \\ \delta \\ \dot{\delta} \end{bmatrix} + \begin{bmatrix} 0 \\ 0 \\ 0 \\ \omega_n^2 \end{bmatrix} \delta_c \qquad (B.42)$$

For the roll dynamics, Eq. (B.8) becomes:

$$\dot{p} = \frac{L}{I_x} \qquad (B.43)$$

Note that L-moment can be expressed in terms of aerodynamic derivatives and some parameteres as in Eq. (B.44):

$$L = L_p p + L_\delta \delta \qquad (B.44)$$

Putting Eq. (B.44) into the Eq. (B.43):

$$\dot{p} = \frac{L_p}{I_x} p + \frac{L_\delta}{I_x} \delta \qquad (B.45)$$

The relationship between Euler angles and body angular rates are as follows [16]:

$$\dot{\phi} = p + q \sin\phi \tan\theta + r \cos\phi \tan\theta \qquad (B.46)$$

With the assumption of $q \approx r \approx 0$:

$$\dot{\phi} = p \qquad (B.47)$$

By adding the CAS dynamics into the system linear matrices for the roll dynamics can be written as in Eq (B.48):

$$\begin{bmatrix} \dot{\phi} \\ \dot{p} \\ \dot{\delta} \\ \ddot{\delta} \end{bmatrix} = \begin{bmatrix} 0 & 1 & 0 & 0 \\ 0 & \frac{L_p}{I_x} & \frac{L_\delta}{I_x} & 0 \\ 0 & 0 & 0 & 1 \\ 0 & 0 & -\omega_n^2 & -2\zeta\omega_n^2 \end{bmatrix} \begin{bmatrix} \phi \\ p \\ \delta \\ \dot{\delta} \end{bmatrix} + \begin{bmatrix} 0 \\ 0 \\ 0 \\ \omega_n^2 \end{bmatrix} \delta_c \qquad (B.48)$$